## ABSTRACT

ZHU, YUWEI. Thermal Neutron Scattering Cross Sections for Silicon Carbide. (Under the direction of Ayman I. Hawari).

Silicon carbide based materials are proposed as a promising fuel and cladding material for fission and fusion applications. While there has been significant research and development work on the manufacturing and determination of radiation effects in SiC, the details of neutron scattering behavior of SiC are still absent. In this situation, neutronics codes such as MCNP will use the default free-gas neutron cross section libraries, which will usually result in significant inaccuracies in the prediction of the neutron spectrum. The predicted thermal spectrum will influence fuel and core design. Therefore, it is important to develop thermal scattering cross section libraries for SiC.

In this work, the scattering cross section libraries for 3C-SiC were fully developed using ab-initio and lattice dynamics methods. Phonon properties of 3C-SiC are estimated by using ab-initio calculated forces for the lattice. Both the coherent elastic and the inelastic cross section in the incoherent approximation are computed and *ENDF/B-VII* libraries are generated. A program was developed for calculating the coherent elastic component that is applicable to all polycrystalline materials. This routine has been implemented into the *LEAPR* module of the *NJOY* code system.

# Thermal Neutron Scattering Cross Sections for Silicon Carbide

by
Yuwei Zhu

A thesis submitted to the Graduate Faculty of
North Carolina State University
in partial fulfillment of the
requirements for the degree of
Master of Science

Nuclear Engineering

Raleigh, North Carolina

2014

APPROVED BY:

_____ _____

Dr. Gail C. McLaughlin Dr. Bernard Wehring

_____

Dr. Ayman I. Hawari
Chair of Advisory Committee

## BIOGRAPHY

Yuwei Zhu was born on February 2, 1990 in Deyang, Sichuan Province, People's Republic of China. Yuwei graduated from No. 5 Middle School of Deyang in 2008 and subsequently enrolled in University of Science and Technology of China. In 2012, he graduated from USTC with Bachelor in Nuclear Engineering. Immediately following graduation, he came to North Carolina State University for his graduate study. Yuwei began working with Dr. Ayman Hawari on the thermal neutron scattering cross section of 3C-SiC as his master research.

## ACKNOWLEDGMENTS

I would like to give my wholehearted gratitude to Dr. Ayman Hawari for guiding me in this project. Without his patients and guidance, this project would be impossible. Dr. Hawari's professional outlook and abundant knowledge always shed light on our discussion. I would like to thank him for supporting me to attend the ANS meeting, where I had a chance to see and listen to others and really learned a lot.

I would also like to thank members of my research group, Jonathan Wormald and Jesse Holmes. Their ample knowledge in nuclear engineering and physics always gives me insight of problems in discussion. Jonathan has been working with me on inelastic cross section. He taught me a lot in research. Jesse's dedication to his career and knowledge of the field inspire me. Many thanks to Dr. Victor Gillette, his knowledge in technical and software issues support me throughout this project.

I would also like to thank my family and friends. Their support gives me determination to overcome obstacles.

## TABLE OF CONTENTS

## LIST OF TABLES

## LIST OF FIGURES

# Chapter 1 Introduction

## 1.1 Overview

Due to its excellent thermal and chemical stability, outstanding mechanical properties, radiation resistance and low activation under neutron irradiation, silicon carbide and its composites are proposed as fuel and structural material in next generation fission and fusion reactors [3]. In the past decade, silicon carbide has enjoyed rising interest in both fundamental modeling and practical experimental study. This thesis focuses particularly on the thermal neutron scattering cross section of SiC material for its development as a nuclear material.

SiC is utilized in nuclear reactor as a fuel material. For example, the fully ceramic microencapsulated (FCM) fuel [4, 5] concept is based on tri-structural isotropic (TRISO) fuel particles embedded in a silicon carbide matrix. SiC is used as supporting matrix as wells as a micro-pressure vessel in TRISO fuel particles. The innermost core of a TRISO fuel particle is the fuel kernel. The neighboring layer is a porous carbon buffer, i.e., low-density pyrolytic carbon (PyC), containing about 50% void. This layer is surrounded by a high-density PyC layer followed by a SiC layer. The outermost layer is a layer of high-density PyC [6]. The SiC layer serves as a barrier to fission product retention as well as a structure layer to prevent the fuel from cracking. This SiC layer is critical to TRISO fuel performance as it renders fuel pebbles the capability of holding the fission production gases in place and withstands stresses from inner layers. Under the FCM design, the graphite matrix is replaced with SiC matrix to offer improved stability, fission product resistance and thermal conductivity.

SiC is also proposed as a cladding material [7, 8]. The unique neutronic and

mechanical properties of zirconium facilitate Zircaloy as a standard material for cladding nuclear fuels. However, due to corrosion and radiation damage of typical cladding materials, fuel rods are often forced to be exchanged before reaching optimum burn up. Investigation suggests that SiC composites have better ability to handle the corrosion and degradation [9]. SiC/SiC composite stands for SiC-matrix reinforced with SiC-fiber. SiC-fibers of high strength are embedded in SiC matrixes which is of lower strength [10]. The fibers offer enough strength for the material while the matrix provides stress transfer and load dispersion. There is also an intermediate layer between fiber and matrix which separates the fiber from the matrix. This layer prevents composite friction and catastrophic failure.

Recent development in SiC enables applications of 4H-SiC as an outstanding microelectronic device material and detection material [11, 12]. Cubic SiC owns a wide bandgap of 2.4 *eV*, while 4H-SiC owns even higher 3.26 *eV* bandgap [13]. Since SiC is more stable under an extreme thermal-chemical environment than Si or C, these microelectronic devices and radiation detectors made from SiC are capable to operate in a hostile environment such as a nuclear reactor.

In the past decades, many methods of fabricating SiC material have been established. Moreover, research reveals that both the non-irradiated and irradiated properties of SiC strongly depend on the fabrication process. In this sense, it is essential to distinguish different material fabrication processes. Methods such as reaction sintering, direct conversion, polymer pyrolysis, nano-infiltration and transient eutectic-phase (NITE), and chemical vapor processing are used in SiC synthesis [6]. Among these available industrial production processes, chemical vapor processing is the most widely used in synthesizing

nuclear-grade SiC and SiC composites.

Chemical vapor processing includes chemical vapor deposition (CVD) and chemical vapor infiltration (CVI) [9]. The CVD process is one of the most commonly used processes to grow monolithic high-purity $\beta$-SiC [14]. This process is basically accumulating SiC onto an oriented crystal surface. The CVI process is used to fabricate the matrix inside the SiC composite [15]. Instead of deposition on a surface, chemical vapor infiltrates between fibers of SiC to form SiC matrix.

Under growing interest of utilizing SiC as a fuel or a core material, evaluation of the operational and safety behavior of the reactor requires accurate nuclear scattering cross section of SiC. Due to the lack of knowledge with this material, all simulations are currently conducted using the free atom cross section of silicon and carbon atoms. In this work, both the inelastic and elastic cross sections of 3C-SiC are produced. The inelastic cross section of 3C-SiC is produced by ab-initio simulation and phonon dynamics matrix method. The coherent elastic cross section is produced with a program developed from basic scattering theory. The cross sections of 3C-SiC are prepared in ENDF/B-VII format which can be easily put into use.

## 1.2 Structure of 3C-SiC

There are currently over 100 polytypes of SiC known to exist. Among these polytypes, only three are commonly used in industry because they are the only polytypes that can be produced in large quantities in bulk single crystal, polycrystalline or fiber/matrix form [9]. One of the three polytypes has a cubic lattice unit cell. It is commonly referred to 3C-

SiC, also known as $\beta$-SiC. Because the lattice of cubic SiC is close packed face centered cubic (fcc), the stacking sequence is denoted as ABCABC… The number 3 in its name herein indicates the number of periodical layers. The other two with hexagonal unit cells are usually called 4H-SiC and 6H-SiC. Because they both have a hexagonally packed layer configuration, they are also collectively referred to $\alpha$-SiC [16]. Of particular interest is 3C-SiC, which is more widely proposed in nuclear reactor as a structure and fuel material [17]. Therefore this thesis will focus only on the discussion of 3C-SiC.

The 3C-SiC form has a face-centered cubic unit cell with a lattice constant of $a$ = 4.3593Å. As shown in Fig. 1, there are 8 atoms in each 3C-SiC unit cell. These atoms are tetragonally bonded to each other and have a coordination number of 4, i.e., there are 4 Si atoms around a C atom and vice versa. The point group of 3C-SiC is $T^2_d$ under Schönflies notation or $F\bar{4}3m$ under Hermann–Mauguin notation.

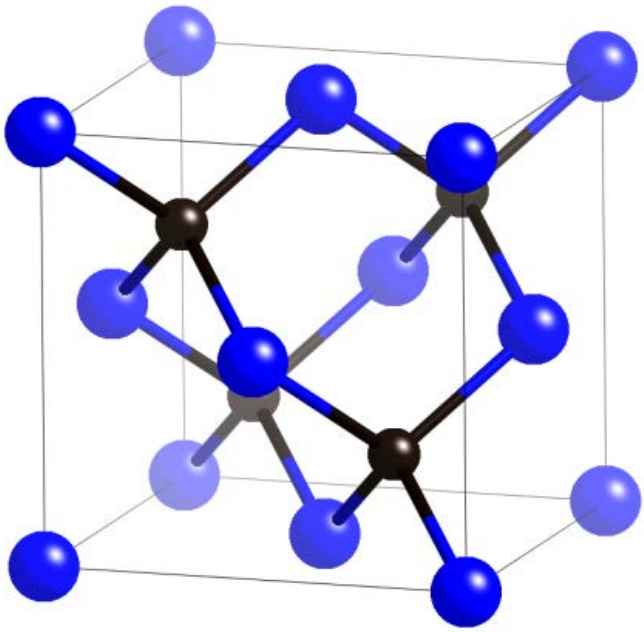

**Fig. 1. Unit cell of 3C-SiC.**

The standard symmetry elements of space group $F\bar{4}3m$ taken from the International Tables of Crystallography are shown in Fig. 2. A detailed compilation of the crystallography terminology can be found in Ref. [18]. This figure is a projection of the $F\bar{4}3m$ unit cell along its ***c*** direction. Four-fold rotoinversion axes are shown to exist on each unit cell edge and diagonals across the body center and face centers. There are four three-fold rotation axes on the body diagonal. Mirror planes are perpendicular to the projection plane on each body diagonal plane. Glide planes and screw axes are also demonstrated in the figure. Since 3C-SiC shows high structural symmetry, *ab-initio* calculation of electronic structure can be efficiently performed.

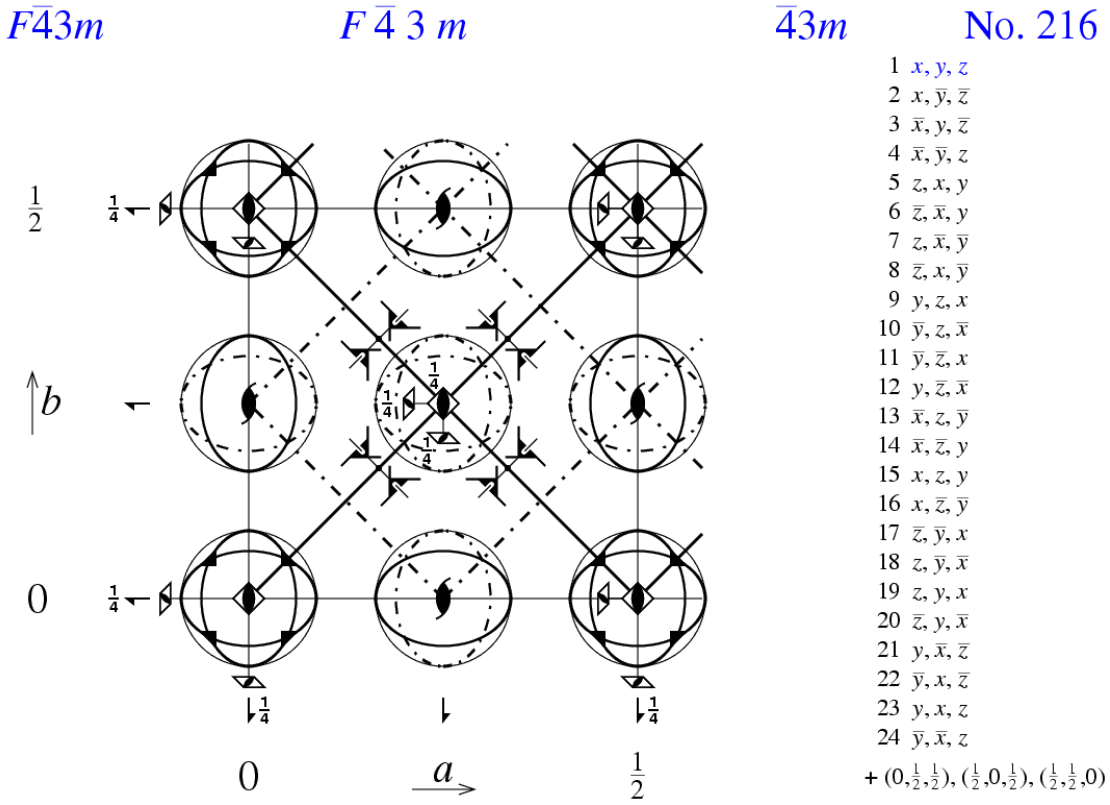


**Fig. 2. Symmetry element of space group $F\bar{4}3m$.**

## 1.3 Nuclear Cross Section

For the purpose of deriving the cross section from predictive methodology, neutrons need to be considered as quantum waves as well as particles. Therefore, in a scattering event, the initial and final neutron wave vectors are assigned $\boldsymbol{k}_i$ and $\boldsymbol{k}_f$. The scattering of a neutron by a sample is characterized by the change of its momentum, $\boldsymbol{P}$, and energy, $E$. Their fundamental relationships with wave vector $\boldsymbol{k}$ are expressed as

$$\mathbf{P} = \hbar\mathbf{k}_\mathbf{i} - \hbar\mathbf{k}_\mathbf{f} = \hbar\boldsymbol{\kappa}\,, \tag{1.1}$$

$$\boldsymbol{\kappa} = \mathbf{k}_\mathbf{i} - \mathbf{k}_\mathbf{f}\,, \tag{1.2}$$

$$E = \frac{\left|\hbar\mathbf{k}_\mathbf{i}\right|^2 - \left|\hbar\mathbf{k}_\mathbf{f}\right|^2}{2m_n}\,. \tag{1.3}$$

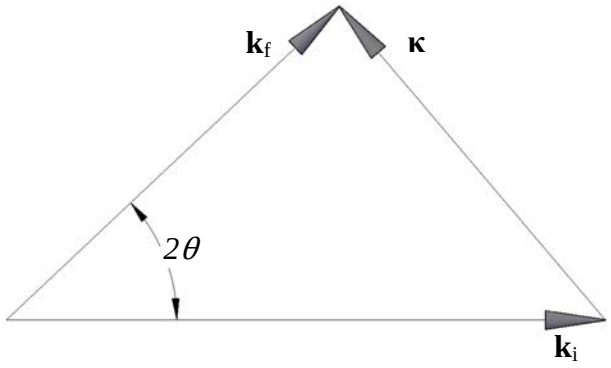


**Fig. 3. Scattering in reciprocal space.**

A steady stream of neutrons of wavelength $\lambda$ traveling in the $z$ direction can be described mathematically by the complex plane wave

$$\psi_i = \psi_0 e^{i\mathbf{k}_\mathbf{i}\cdot\mathbf{z}} \tag{1.4}$$

with $\psi_0 = \left|\psi_0\right| e^{i(\phi_0 - \omega t)}$, where the incident flux $\Phi = \left|\psi_0\right|^2$, $k_i = 2\pi/\lambda$. The general expression

for the scattered wave in quantum mechanics is

$$\psi_f = -\psi_0 b \frac{e^{i\mathbf{k}_f \cdot \mathbf{r}}}{r}, \tag{1.5}$$

in which the quantity $b$ in $\psi_f$ is known as the scattering length.

Now consider a beam of thermal neutrons incident on a target. The target is a general collection of atoms. The scattering system could be gas, liquid, a crystal or an amorphous material. Incoming neutrons are scattered out of the target in all $4\pi$ directions with all possible energies, as shown in Fig. 4. Suppose a perfect neutron spectrometer is set up in a particular direction. The distance of the spectrometer from the scattering system is large compared to the dimension of target, thus the spectrometer subtends only a small solid angle $d\Omega$. The spectrometer counts all neutrons within a certain energy range from $E'$ to $E'+dE'$.

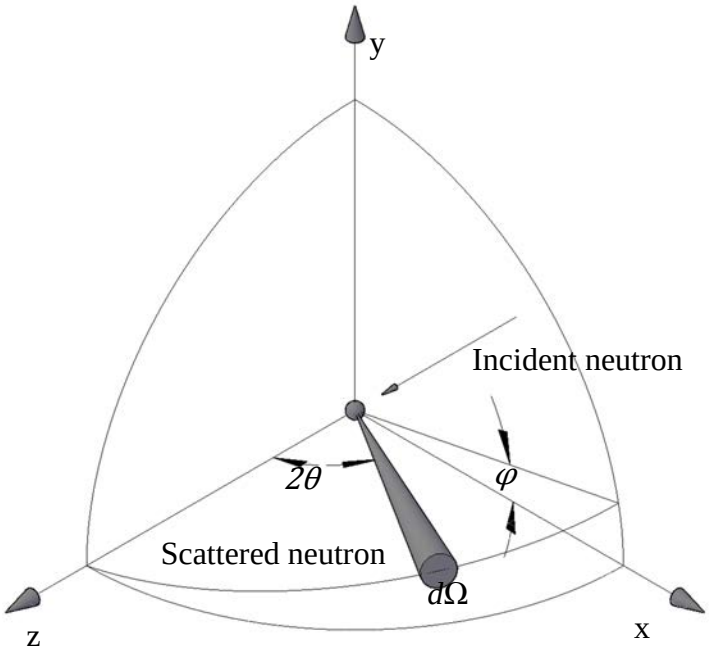


**Fig. 4. The Neutron scattering system.**

The double-differential cross section [19] is defined by

$$\frac{d^2\sigma}{dE'd\Omega} = \frac{\begin{array}{c}\text{number of neutrons scattered into the direction } 2\theta,\varphi \text{ within} \\ \text{solid angle } d\Omega \text{ with energy between } E' \text{ and } E'+dE' \text{ per second}\end{array}}{\Phi d\Omega dE'}, \qquad (1.6)$$

where $\Phi$ is the flux of the incident neutrons, which is given by the multiplication of the velocity and neutron density. It should be noted that the double differential cross section is sometimes also called a partial differential cross section. The differential cross section is defined as

$$\frac{d\sigma}{d\Omega} = \frac{\begin{array}{c}\text{number of neutrons scattered into direction} \\ 2\theta,\varphi \text{ within solid angle } d\Omega \text{ per second}\end{array}}{\Phi d\Omega dE'}. \qquad (1.7)$$

This cross section is measured by a neutron diffractometer, which counts the number of neutrons regardless of the scattered neutron energy. The total cross section is an integral of differential cross sections over all $4\pi$ direction. It is given by

$$\sigma_{tot} = \frac{\text{number of neutrons scattered in all directions per second}}{\Phi}. \qquad (1.8)$$

The differential and total cross section hence is

$$\frac{d\sigma}{d\Omega} = \frac{\iint |\psi_f|^2 dA}{|\psi_i|^2 d\Omega} = b^2, \qquad (1.9)$$

$$\sigma_{tot} = 4\pi b^2, \qquad (1.10)$$

where $b$ is the scattering length in equation (1.5).

# Chapter 2 Thermal Neutron Scattering

In this chapter, a derivation of an expression that describes the neutron scattering cross section will be established. To start the derivation, the Born approximation will be applied. The scattering potential of a neutron versus a nucleus is assumed to be Fermi's pseudopotential. Based on the two basic approximations above, a computationally friendly expression will be derived. Interpretations and discussions of important parameters such as Debye-Waller factor and scattering law are made.

## 2.1 Derivation of the Scattering Cross Section from First Principles

The derivation of thermal neutron scattering cross sections is majorly adopted from Ref. [20]. Consider a scattering process in which the state of the scattering target changes from $\lambda$ to $\lambda'$, and the state of neutrons change from $k$ to $k'$. The cross section in this particular scenario is given by

$$\left(\frac{d\sigma}{d\Omega}\right)_{\lambda\to\lambda'} = \frac{1}{\Phi}\frac{1}{d\Omega}\sum_{k' \text{ in } d\Omega} W_{k,\lambda\to k',\lambda'}, \tag{2.1}$$

where $W_{k,\lambda\to k',\lambda'}$ is the number of transitions from the state $k$, $\lambda$ to the state $k'$, $\lambda'$. To make the formula of the cross section derivable, as the first step, the Born approximation from first order time dependent perturbation theory is applied. $W_{k,\lambda\to k',\lambda'}$ is obtained analytically as

$$\sum_{k' \text{ in } d\Omega} W_{k,\lambda\to k',\lambda'} = \frac{2\pi}{\hbar}\rho_{k'}\left|\left\langle k',\lambda'\middle|V\middle|k,\lambda\right\rangle\right|^2, \tag{2.2}$$

where $\rho_{k'}$ is the number of momentum states in $d\Omega$ per unit energy range for neutrons in the states $k'$, $V(\mathbf{r})$ is the nuclear potential from which a neutron scatters away. As the second step

to obtain an analytical formula for cross section, $V(\mathbf{r})$ is approximated as Fermi's pseudopotential

$$V(\mathbf{r}) = \frac{2\pi\hbar^2}{m} b\delta(\mathbf{r}) . \tag{2.3}$$

The δ-function comes from the concept that the interaction range of the nucleus potential is short compare to the scale of atom ($1\times10^{-10}\,m$). As a neutral particle, a neutron interacts with the nucleus through the strong nuclear force. The range of the strong nuclear force, which extends only to the order of femtometer ($1\times10^{-15}\,m$), allows the use of a δ-function to represent the potential.

Inserting these values back into (2.1) along with some mathematical treatment will give

$$\left(\frac{d^2\sigma}{d\Omega dE'}\right)_{\lambda\to\lambda'} = \frac{k}{k'}\frac{1}{2\pi\hbar}\sum_{jj'} b_{j'}b_j \int_{-\infty}^{\infty} \left\langle \lambda \left| e^{-i\boldsymbol{\kappa}\cdot\mathbf{R}_{j'}} \right| \lambda' \right\rangle \left\langle \lambda' \left| e^{iHt/\hbar} e^{i\boldsymbol{\kappa}\cdot\mathbf{R}_j} e^{-iHt/\hbar} \right| \lambda \right\rangle e^{-i\omega t} dt . \tag{2.4}$$

The subscript $\lambda\to\lambda'$ in the double differential cross section indicates that the scattering cross section is for the specific case when the system is changing from state $\lambda$ to $\lambda'$. Obtaining Eq. (2.4) means that the Born approximation and Fermi's pseudopotential will be implicitly implied in all of our later formulas. In application, the scattering system is an assembly of atoms in which the probability of finding an atom with energy $E$ adheres to the Boltzmann distribution. After scattering, the final states of atoms are determined by quantum mechanics. Accordingly, to evaluate the double differential scattering cross section, all the final states $\lambda'$ need to be sum over and averaged over all the possible initial states $\lambda$. In order to achieve this goal, the Boltzmann distribution and Heisenberg operators are applied,

$$\frac{d^2\sigma}{d\Omega dE'} = \frac{k}{k'}\frac{1}{2\pi\hbar}\sum_{jj'} b_{j'} b_j \int_{-\infty}^{\infty} \left\langle e^{-i\boldsymbol{\kappa}\cdot\mathbf{R}_{j'}(0)} e^{i\boldsymbol{\kappa}\cdot\mathbf{R}_j(t)} \right\rangle e^{-i\omega t} dt \,, \tag{2.5}$$

in which the $\mathbf{R}_j(t)$ is the Heisenberg notation of atom position

$$\mathbf{R}_j(t) = e^{iHt/\hbar}\mathbf{R}_j e^{-iHt/\hbar} \,. \tag{2.6}$$

The average notation in (2.5) of all the initial states of the system is denoted by

$$\langle A \rangle = \sum_{\lambda} p_\lambda \langle \lambda | A | \lambda \rangle \,, \tag{2.7}$$

where $p_\lambda$ is the probability of state $\lambda$ in Boltzmann distribution. Equation (2.5) is the most compact form for the double-differential cross section. Information about the potential of a scattering system is contained in the Hamiltonian *H*, which is contained in a Heisenberg operator. Properties of the cross section of each nucleus in the scattering system are given in the summation of $b_j$, as defined in Eq. (1.5). Energy information about the incident and scattered neutron is included in *k* and *k′*. Direction information of the scattering is incorporated in $\boldsymbol{\kappa}$.

Further evaluations of the cross section will originate from this expression. However, before proceeding to evaluate Eq. (2.5), a separation of the coherent and incoherent cross section should be made. This separation can be comprehended physically and later evaluation will benefit from it.

The scattering length is a physical attribute to each isotope of every chemical element. Moreover, nuclei with different spin states also have different scattering lengths. For example, if a nucleus has a spin up (+) state and a spin down (-) state, these states will have scattering lengths b+ and b-, respectively. Hence, the scattering system is quite often a

mixture of isotopes with different scattering lengths.

Consider Eq. (2.5), if it is written that

$$\sum_{j',j} b_{j'} b_j = \sum_{j',j} \overline{b_{j'} b_j} = \overline{b^2} + \bar{b}^2, \tag{2.8}$$

where $\overline{b^2} = \overline{b_j b_{j'}},\ j' = j$ ; $\bar{b}^2 = \overline{b_j}\,\overline{b_{j'}} = \overline{b_j b_{j'}},\ j' \neq j$ . Thus Eq. (2.5) can be expressed in two terms:

$$\frac{d^2\sigma}{d\Omega dE'} = \frac{k'}{k}\frac{1}{2\pi\hbar}\bar{b}^2 \sum_{jj'} \int \langle j', j \rangle e^{-i\omega t} dt + \frac{k'}{k}\frac{1}{2\pi\hbar}\left(\overline{b^2} - \bar{b}^2\right)\sum_j \int \langle j, j \rangle e^{-i\omega t} dt . \tag{2.9}$$

The first summation in Eq. (2.9) represents the coherent scattering cross section, in which the waves scattered from each nucleus interfere with each other. The physical interpretation of the coherent cross section is the cross section of a scattering system which consists of nuclei with single scattering length $\bar{b}$. The second summation is known as the incoherent cross section. It does not give rise to any interference between nuclei. Moreover, its magnitude is completely determined by the mean square deviation of scattering length from the average value. It can be written that

$$\left(\frac{d^2\sigma}{d\Omega dE'}\right)_{coh} = \frac{\sigma_{coh}}{4\pi}\frac{k'}{k}\frac{1}{2\pi\hbar}\sum_{jj'}\int_{-\infty}^{\infty}\left\langle e^{-i\boldsymbol{\kappa}\cdot\mathbf{R}_{j'}(0)} e^{i\boldsymbol{\kappa}\cdot\mathbf{R}_j(t)}\right\rangle e^{-i\omega t} dt , \tag{2.10}$$

$$\left(\frac{d^2\sigma}{d\Omega dE'}\right)_{inc} = \frac{\sigma_{inc}}{4\pi}\frac{k'}{k}\frac{1}{2\pi\hbar}\sum_{j}\int_{-\infty}^{\infty}\left\langle e^{-i\boldsymbol{\kappa}\cdot\mathbf{R}_{j}(0)} e^{i\boldsymbol{\kappa}\cdot\mathbf{R}_j(t)}\right\rangle e^{-i\omega t} dt , \tag{2.11}$$

where $\sigma_{coh} = 4\pi\langle b\rangle^2$ , $\sigma_{inc} = 4\pi\left(\langle b^2\rangle - \langle b\rangle^2\right)$.

It can be seen that Eq. (2.10) gives correlation between every atom in the summation. On the other hand, the equation of incoherent scattering, Eq. (2.11), gives only the

correlation of a single atom with different time. Thus it is said that coherent scattering contributes to interference effects and yields space and time correlations. Incoherent scattering does not contain interference information. It arises from the random distribution of scattering lengths and their deviation from the average scattering length.

## 2.2 Theory of inelastic scattering cross section

By combining Eq. (2.10) and Eq. (2.11) together, the scattering cross section can be written in a compact way

$$\frac{d^2\sigma}{d\Omega dE'} = \frac{1}{4\pi}\frac{k'}{k}\left(\sigma_{coh}S(\boldsymbol{\kappa},\omega) + \sigma_{inc}S_s(\boldsymbol{\kappa},\omega)\right), \tag{2.12}$$

where $S(\boldsymbol{\kappa},\omega)$ is known as the scattering law, i.e., the dynamic structure factor. The scattering law denotes the dynamic information from the scattering system, independent of incoming neutron properties. $S(\boldsymbol{\kappa},\omega)$ is made up of self and distinct terms [21, 22] and can be written as

$$S(\boldsymbol{\kappa},\omega) = S_s(\boldsymbol{\kappa},\omega) + S_d(\boldsymbol{\kappa},\omega). \tag{2.13}$$

By comparing Eq. (2.10) and Eq. (2.11) with Eq. (2.13), the self and distinct scattering law should correspond to

$$S_d(\boldsymbol{\kappa},\omega) = \frac{1}{2\pi\hbar}\sum_{jj',j\neq j'}\int_{-\infty}^{\infty}\left\langle e^{-i\boldsymbol{\kappa}\cdot\mathbf{R}_{j'}(0)}e^{i\boldsymbol{\kappa}\cdot\mathbf{R}_j(t)}\right\rangle e^{-i\omega t}dt, \tag{2.14}$$

$$S_s(\boldsymbol{\kappa},\omega) = \frac{1}{2\pi\hbar}\sum_{j}\int_{-\infty}^{\infty}\left\langle e^{-i\boldsymbol{\kappa}\cdot\mathbf{R}_j(0)}e^{i\boldsymbol{\kappa}\cdot\mathbf{R}_j(t)}\right\rangle e^{-i\omega t}dt. \tag{2.15}$$

As can be shown here, the scattering law is basically Fourier transform of the atomic spatial

distribution (which is contained in the average notation as shown in Eq. (2.7)). In the case when the harmonic approximation is introduced, where interatomic forces are proportional to displacement from equilibrium position, the scattering law in a crystal can be further expanded as

$$S_s = {}^0S_s + {}^1S_s + {}^2S_s + {}^3S_s + \ldots, \tag{2.16}$$

$$S_d = {}^0S_d + {}^1S_d + {}^2S_d + {}^3S_d + \ldots. \tag{2.17}$$

This is known as the phonon expansion, where the superscript represents number of phonons created or annihilated. For example, the 0 term corresponds to elastic scattering while the 1 term corresponds to the situation where one phonon is excited or deexcited.

To calculate the inelastic cross section in a crystal material, the incoherent approximation is introduced. The incoherent approximation assumes that the distinct scattering law $S_d$ is small compared to the self-scattering law $S_s$, in another word, $S_d = 0$. By ignoring the contribution of distinct scattering law $S_d$, Eq. (2.12) can be written as the following form using phonon expansion

$$\left(\frac{d^2\sigma}{d\Omega dE'}\right)_{ine} = \frac{\sigma}{4\pi}\frac{k'}{k}\sum_{n>0}{}^nS_s(\mathbf{Q},\omega), \tag{2.18}$$

where $\sigma = \sigma_{coh} + \sigma_{inc}$. The comparison of bound coherent and bound incoherent scattering cross section for Si and C atom is shown in Table 1.

Table 1. Bound coherent and incoherent scattering cross section for C and Si atom.

| Element | $\sigma_{coh}$ /barn | $\sigma_{inc}$ /barn | $\sigma$ /barn |
|---|---|---|---|
| C | 5.551 | 0.001 | 5.551 |
| Si | 2.163 | 0.004 | 2.167 |

Therefore, it is safe to say that $\sigma \approx \sigma_{coh}$ in the case of silicon carbide. That is to say, for inelastic scattering cross section under incoherent approximation, the major contribution of the cross section comes from $\sigma_{coh}$. It should also be emphasized that the incoherent approximation only renders distinct scattering law $S_d$ to be zero. It made no assumption on the significance of the contribution from bound incoherent cross section $\sigma_{inc}$.

## 2.3 Theory of Coherent Elastic Scattering Cross Section

The corresponding equation for coherent scattering expressed by the scattering law is

$$\left(\frac{d^2\sigma}{d\Omega dE'}\right)_{coh} = \frac{\sigma_{coh}}{4\pi}\sqrt{\frac{E'}{E}}({}^0S + {}^1S + \ldots). \tag{2.19}$$

The coherent elastic scattering cross section is obtained by ignoring all the phonon generation or annihilation terms. That is to say, in Eq. (2.19), only the ${}^0S_d$ and ${}^0S_s$ terms are left for elastic scattering,

$$\left(\frac{d^2\sigma}{d\Omega dE'}\right)_{coh} = \frac{\sigma_{coh}}{4\pi}\,{}^0S. \tag{2.20}$$

Therefore, the goal of this section is to derive an expression for the elastic scattering law term ${}^0S$.

As an easier strategy to deduce a computational expression for coherent elastic cross section, firstly a Bravais crystal is assumed and then a non-Bravais crystal formula will be developed. To proceed to evaluate Eq. (2.20), an analytic expression of atom position $\boldsymbol{R}_j(t)$ must be obtained. $\boldsymbol{u}_l(t)$ is assigned as the atomic displacement and $\boldsymbol{l}$ as the atomic

equilibrium position. Therefore, in a Bravais crystal, it can be written that

$$\mathbf{R}_j(t) = \mathbf{l} + \mathbf{u}_l(\mathrm{t}). \tag{2.21}$$

So in Eq. (2.10), the correlation term can be put as

$$\sum_{ll'} \left\langle e^{-i\boldsymbol{\kappa}\cdot\mathbf{R}_{l'}(0)} e^{i\boldsymbol{\kappa}\cdot\mathbf{R}_l(t)} \right\rangle = N \sum_{l} e^{i\boldsymbol{\kappa}\cdot\mathbf{l}} e^{-i\boldsymbol{\kappa}\cdot\mathbf{u}_0(0)} e^{i\boldsymbol{\kappa}\cdot\mathbf{u}_l(\mathrm{t})} \,. \tag{2.22}$$

The summation is started from $\boldsymbol{l'}$ =0, because in a crystal system, transformation symmetry enables us to use relative position $\boldsymbol{l - l'}$ to determine all the positions in the crystal regardless of the value of $\boldsymbol{l'}$.

In order to achieve our goal to analytically express $\boldsymbol{R}_j(t)$, the next step is to assume that interatomic potential in the crystal system is harmonic, i.e., forces are proportional to displacements from each atom's equilibrium position. This is only true when atoms are vibrating at a relative small range compared to their lattice constant. The harmonic potential approximation is a basis of phonon theory from solid state physics. It renders us the capability to calculate theoretical values of physical properties, including the cross section, utilizing phonons. The main justification for this is the already successful predictions of many of the observed properties and predictions. In the particular situation of SiC, 3C-SiC as a semiconductor material lacks electrons in conduction band. The internal energy carrier in SiC, therefore, is majorly phonon.

In order to proceed to evaluate elastic cross section using phonon expansion in Eq. (2.16) and Eq. (2.17), model of quantum harmonic oscillator is applied. By considering every atom as a quantum harmonic oscillator, $\boldsymbol{u}_l$ can be found in most quantum texts as

$$\mathbf{u}_l = \sqrt{\frac{\hbar}{2MN}} \sum_s \frac{\mathbf{e}_s}{\sqrt{\omega_s}} \left( a_s e^{i\mathbf{q}\cdot\mathbf{l}} + a_s^{\dagger} e^{-i\mathbf{q}\cdot\mathbf{l}} \right), \tag{2.23}$$

where $\boldsymbol{q}$ is its wave vector, $\boldsymbol{e}_s$ is its polarization vector, $s$ indexes both $\boldsymbol{q}$ and polarization index (*1*,*2*,*3*). For another word, the sum of $s$ is over $N$ points of $\boldsymbol{q}$ in the first Brillouin zone and 3 polarization directions. $a_s$ and $a_s^{\dagger}$ stand for the annihilation operator and the creation operator for the state $s$. The time dependent displacement $\boldsymbol{u}_l(t)$ can be expressed by Heisenberg operator which will eventually operate on $a_s$ and $a_s^{\dagger}$.

$$a_s(t) = e^{iHt/\hbar} a_s e^{-iHt/\hbar}, \tag{2.24}$$

$$a_s^{\dagger}(t) = e^{iHt/\hbar} a_s^{\dagger} e^{-iHt/\hbar}. \tag{2.25}$$

If not stated explicitly, both $a_s$ and $a_s^{\dagger}$ shall stand for the time dependent $a_s(t)$ and $a_s^{\dagger}(t)$ from now on. Another set of short-hand notations that is applied is

$$U = -i\boldsymbol{\kappa}\cdot\mathbf{u}_0(0) = -\mathrm{i}\sum_s g_s a_s + g_s a_s^{\dagger}, \tag{2.26}$$

$$V = i\boldsymbol{\kappa}\cdot\mathbf{u}_l(\mathrm{t}) = \mathrm{i}\sum_s h_s a_s + h_s^{*} a_s^{\dagger}, \tag{2.27}$$

$$g_s = \sqrt{\frac{\hbar}{2MN}} \frac{\boldsymbol{\kappa}\cdot\mathbf{e}_s}{\sqrt{\omega_s}}, \tag{2.28}$$

$$h_s = \sqrt{\frac{\hbar}{2MN}} \frac{\boldsymbol{\kappa}\cdot\mathbf{e}_s}{\sqrt{\omega_s}} e^{i(\mathbf{q}\cdot\mathbf{l}-\omega_s t)}. \tag{2.29}$$

By substituting Eq. (2.21) ~ (2.29) into Eq. (2.10), after somewhat lengthy calculation

$$\left(\frac{d^2\sigma}{d\Omega dE'}\right)_{coh} = \frac{\sigma_{coh}}{4\pi}\frac{k'}{k}\frac{N}{2\pi\hbar} e^{\langle U^2\rangle} \sum_l e^{i\boldsymbol{\kappa}\cdot\mathbf{l}} \int_{-\infty}^{\infty} e^{\langle UV\rangle} e^{-i\omega t} dt. \tag{2.30}$$

If the term $e^{\langle UV\rangle}$ in Eq. (2.30) is Taylor expanded,

$$e^{\langle UV\rangle} = 1 + \langle UV\rangle + \frac{1}{2!}\langle UV\rangle^2 + \ldots + \frac{1}{p!}\langle UV\rangle^p + \ldots, \tag{2.31}$$

in which the very first term gives the elastic scattering process and the rest term with $p^{\text{th}}$ power gives p-phonon process. The p-phonon terms contribute only a small portion to the total coherent cross section of 3C-SiC. Hence of particular interest is the elastic scattering process in our research. Therefore, theoretical deduction will be proceeded only with the elastic term in Eq. (2.31). By replacing $e^{\langle UV\rangle}$ with 1 and apply the $k=k'$ relation in elastic scattering, the differential coherent elastic cross section will follow by integral of $E'$ over all scattered neutron energy

$$\left(\frac{d\sigma}{d\Omega}\right)_{coh\ el} = \frac{\sigma_{coh}}{4\pi} N e^{\langle U^2\rangle} \sum_l e^{i\boldsymbol{\kappa}\cdot\mathbf{l}}. \tag{2.32}$$

With the periodicity of crystal lattice, the summation of $\boldsymbol{l}$ can be largely simplified as a δ-function, which changes the coherent elastic cross section to

$$\left(\frac{d\sigma}{d\Omega}\right)_{coh\ el} = \frac{\sigma_{coh}}{4\pi} N \frac{(2\pi)^3}{v_0} e^{-2W} \sum_{\boldsymbol{\tau}} \delta(\boldsymbol{\kappa} - \boldsymbol{\tau}), \tag{2.33}$$

where $N$ is the number of unit cells in the crystal. The δ-function $\delta(\boldsymbol{\kappa}\text{-}\boldsymbol{\tau})$ is the Bragg's law, i.e., $n\lambda = 2d\sin\theta$, written in reciprocal space. It should be noted that because Eq. (2.10) and Eq. (2.22) are summing over all the atoms in the scattering system, in this case a crystal, the coefficient $N$ should be taken off for the cross section of a single unit cell. The exponential term $e^{-2W}$ is called the Debye-Waller factor, which is of paramount importance in our cross-section calculation. The exponential term $2W = -\langle U^2\rangle = \langle\{\boldsymbol{\kappa}\cdot\mathbf{u}_0(0)\}^2\rangle$ is called Debye-Waller coefficient.

Equation (2.33) is derived from the first principle based on several approximations. However, readers may find it hard to interpret the physics meaning behind each term. An easier approach is offered by Ref. [23] and extended in Appendix A. This methodology of derivation may help readers comprehend how the physics is built into each equation.

The derivation of the coherent elastic cross section for non-Bravais crystal follows the same philosophy as Eq. (2.33). Since, for a non-Bravais crystal, there are more than one atom per unit cell, the cross section should take into account all the atom positions in a unit cell. This leads to

$$\left(\frac{d\sigma}{d\Omega}\right)_{coh\ el} = N\frac{(2\pi)^3}{v_0}\sum_{\boldsymbol{\tau}}\delta(\boldsymbol{\kappa}-\boldsymbol{\tau})\left|F(\boldsymbol{\kappa})\right|^2 \tag{2.34}$$

where $F(\boldsymbol{\kappa})$ is known as the *nuclear structure factor*.

$$F(\boldsymbol{\kappa}) = \sum_{\mu}\overline{b}_{\mu}e^{i\boldsymbol{\kappa}\cdot\mathbf{d}}e^{-W_{\mu}} \tag{2.35}$$

in which $W_{\mu}$ is the Debye-Waller coefficient of atom $\mu$ in a non-Bravais crystal.

## 2.4 Derivation of Debye-Waller Factor

As shown in Eq. (2.32) and Eq. (2.33), Debye-Waller factor $e^{-2W} = e^{\langle U^2\rangle}$ is the exponential of the mean square displacement along the $\boldsymbol{\kappa}$ direction. In another word, in a crystal system, Debye-Waller factor takes into account of thermal oscillation of atoms around their equilibrium positions and their zero point energy. Calculating Debye-Waller factor is one of the most important steps to correctly evaluate the cross section. For the convenience of writing a program, there are some approximations that should be made on crystalline

materials for Debye-Waller factor.

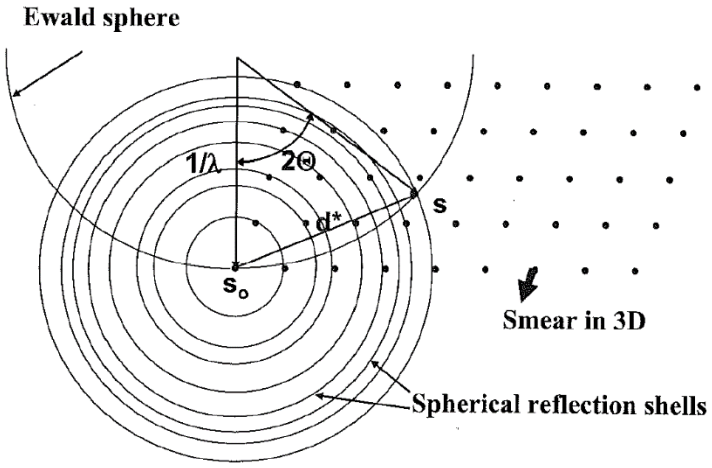


**Fig. 5. Reciprocal space construction for a powder scattering experiment.**

In a polycrystalline material where the dimension of randomly orientated crystal mosaic is small enough, it can be assumed that the incident neutron beam is able to "see" all crystal directions. Thus, in reciprocal space, spherical reflection shells are constructed by randomly orientated lattice points. These spheres are isotropic to incoming neutron direction (please refer to Fig. 5).

This isotropic symmetry of incident neutron beam can also be obtained in case of a single crystal made up of cubic unit cells. Therefore, the expression for the Debye-Waller factor of a polycrystalline material is exactly the same as that of a single cubic crystal. From historical convention, this assumption of using isotropic symmetry to calculate Debye-Waller factor is called *cubic approximation.* In the field of nuclear engineering, almost all nuclear materials used in reactor are polycrystalline materials. Therefore, it is safe to apply the cubic approximation on any crystalline materials used in nuclear engineering. After the cubic

approximation is applied, the Debye-Waller coefficient in Eq. (2.33) for a polycrystalline material is

$$2W = \frac{\hbar \boldsymbol{\kappa}^2}{2M} \int_0^{\omega_m} \frac{\rho(\omega)}{\omega} \coth\left(\frac{\hbar\omega}{2k_B T}\right) \mathrm{d}\omega , \tag{2.36}$$

where $\rho(\omega)$ implies the phonon density of states (DOS). The phonon DOS gives probability density of modes available at frequency $\omega$. It should be noted that $\rho(\omega)$ should be normalized so that integral over all frequencies equals to 1 before applied in Eq. (2.36):

$$\int \rho(\omega) d\omega = 1 . \tag{2.37}$$

Since Eq. (2.33) is derived under Bravais crystal assumption, Eq. (2.36) holds only for Bravais polycrystalline materials. However, in case of non-Bravais crystal, as appeared in Eq. (2.35), the Debye-Waller coefficient should be

$$W_\mu = \frac{\hbar \boldsymbol{\kappa}^2}{4M_\mu} \int_0^{\omega_m} \frac{\rho(\omega)}{\omega} \coth\left(\frac{\hbar\omega}{2k_B T}\right) \mathrm{d}\omega . \tag{2.38}$$

As shown here, instead of having a universal Debye-Waller coefficient for the whole unit cell, $W_\mu$ is calculated at each atom position in a unit cell.

To sum up, there are two approximations applied in Eq. (2.36) and Eq. (2.38). The first one is that displacements of atoms are independent of lattice sites and atom types. This means for every atom in the scattering system, its displacement is isotropic in all directions, i.e.,

$$2W = \overline{(\boldsymbol{\kappa} \cdot \mathbf{u})^2} = \boldsymbol{\kappa}^2 \overline{\mathbf{u}_{\boldsymbol{\kappa}}{}^2} = 1/3 \kappa^2 \overline{u^2} . \tag{2.39}$$

The benefit of this assumption is that a universal DOS $\rho(\omega)$ instead of several different partial DOS can be applied to evaluate a universal value of Debye-Waller factor. However,

this is not always true due to existence of off-diagonal DOS resulting from non-homogeneous forces in the crystal.

The second assumption applied, as mentioned above, is the cubic approximation. However, in the situation of a non-cubic single crystal material, the cubic approximation cannot be applied. Or in a directionally oriented material, e.g., lamellar structure graphite composed by two-dimension layers, the approximation cannot be applied either. In this case, the polarization of phonon modes is no longer symmetric. In the above cases, a more specific Debye-Waller factor shall be used. This Debye-Waller factor is illustrated below.

Recall that in Eq. (2.38), it uses total DOS $\rho(\omega)$, which is the summation of partial DOS. In a more general theory, the DOS is a 3×3 matrix. The partial DOS are phonon DOS on three Cartesian polarization directions $\rho(x)$, $\rho(y)$, $\rho(z)$ locating on the diagonal of the DOS matrix. They describe the contribution from different polarization direction to the total phonon DOS. They are defined as

$$\rho_{i,\mu}(\omega) = \frac{1}{nd\Delta\omega} \sum_{\mathbf{k},j} \left| e_i(\mathbf{k}, j; \mu) \right|^2 \delta_{\Delta\omega}(\omega - \omega(\mathbf{k}, j)), \tag{2.40}$$

where $e_i(\boldsymbol{k}, j; \mu)$ is the $i^{th}$ Cartesian component of the polarization vector for the $\mu^{\text{th}}$ particle in the unit cell, $\omega(\boldsymbol{k}, j)$ is the phonon frequency, and $d$ is the dimension of the dynamical matrix. Moreover, there are also off-diagonal DOS which are defined as

$$\rho_{il,\mu}(\omega) = \frac{1}{nd\Delta\omega} \sum_{\mathbf{k},j} e_i(\mathbf{k}, j; \mu) e_l^*(\mathbf{k}, j; \mu) \delta_{\Delta\omega}(\omega - \omega(\mathbf{k}, j)). \tag{2.41}$$

The off-diagonal terms denotes the correlation between phonons polarized in three orthogonal directions. Combined with diagonal terms, the phonon DOS can be written as a

3×3 matrix. If there is no correlation between forces along *x*, *y*, *z* directions in the crystal, the off-diagonal terms should be zeros. However, due to different kinds of crystal symmetry and different electron distribution of chemical elements, the forces are not always isotropic in the crystal. That is to say, the off-diagonal terms are not always zeros. For example, in cubic lattice (3C-SiC is this case) they are in orders of magnitude smaller than the diagonal terms. Hence, it is safe to apply the isotropic approximation and only consider the existence of partial DOS. In the cases of randomly oriented polycrystalline materials and single cubic crystal, this approximation holds. But in the situation of a single crystal with correlation between forces along *x*, *y*, *z* directions, the matrix of phonon DOS should be applied to calculate the Debye-Waller factor. It should be noted again that phonon DOS should be normalized before applied to calculate the Debye-Waller factor.

Now the Debye-Waller matrix $\mathbf{B}(\mu)$ can be calculated using the phonon DOS matrix. Elements of the 3×3 matrix $\mathbf{B}(\mu)$ represent the mean square displacement of an atom $\mu$ in each direction and their correlation. It is expressed as

$$B_{il}(\mu) = \frac{\hbar}{2M_\mu}\int_0^{\omega_m} \frac{\rho_{il,\mu}(\omega)}{\omega}\coth\left(\frac{\hbar\omega}{2k_BT}\right)\mathrm{d}\,\omega\,. \tag{2.42}$$

The Debye-Waller coefficient is then

$$W_\mu = \frac{1}{2}\boldsymbol{\tau}\cdot\mathbf{B}(\mu)\cdot\boldsymbol{\tau} \tag{2.43}$$

The new Debye-Waller factor then can be plugged into Eq. (2.35) to calculate nuclear structure factor.

# Chapter 3 Computational method

The theories of coherent elastic and inelastic cross section are fully proposed in Chapter 2. In this chapter, methods on how to apply these theories to calculate the cross sections will be described. Important algorithms concerning Debye-Waller factor and coherent elastic cross section will also be discussed.

## 3.1 Computation of Coherent Elastic Scattering Cross Section

For application purpose, our calculated cross section will be processed and published using ENDF/B-VII format. Therefore, a good choice is to implement our program into the existing nuclear data processing code, i.e., *NJOY* [24, 25] in this research. However, the *LEAPR* module in *NJOY* uses a different set of nomenclature from what is shown beforehand. A transformation from the standard terminology to *NJOY* form, therefore, is necessary (shown in Appendix B). In this work, a set of program-friendly equations will be derived and applied. The sections below will try to demonstrate the philosophy of how they are applied in our program.

As mentioned in Section 2.3, there are different strategies that can be applied to calculate the Debye-Waller factor when different approximations are applied.

### 3.1.1 Coherent Elastic Scattering Cross Section with Cubic Approximation

Cross section is the final station of our trip. Thus to reach it, calculation of Debye-Waller factor should be the first stop. As shown in Eq. (2.38), when the cubic approximation

is applied, there is an universal Debye-Waller factor for all atom types. The calculation of Debye-Waller factor is carried out as shown below:

$$\lambda = \int_0^\infty \frac{1}{\beta} \rho(\beta) \coth(\frac{\beta}{2}) d\beta , \tag{3.1}$$

$$w_\mu = \frac{\lambda}{Ak_B T} , \tag{3.2}$$

$$w = \sum_\mu w_\mu \frac{n_\mu}{n_{tot}} , \tag{3.3}$$

where $\alpha = \frac{E' + E - 2m_n\sqrt{E'E}}{Ak_B T}$ is the unitless momentum transfer, $\beta = \frac{E' - E}{k_B T}$ is the unitless energy transfer, $A$ is the atom mass in *amu*, $k_B$ is the Boltzmann Constant and $T$ is the temperature. This calculation routine is essentially the same as the one proposed by Squires in Eq. (2.38). The prof can be found in Appendix B. As shown in Eq. (3.3), universal Debye-Waller coefficient is a summation over each atom type weighted by corresponding atomic ratio. It should be mentioned that the exact value of $A$ input into the program should be the mass ratio of atom $\mu$ to neutron. However, it is still a good approximation to just use $A$ as atomic mass in *amu*, errors are negligible.

The integral of $\beta$ which gives $\lambda$ is accomplished in two steps in the program. In the first step, the phonon DOS is divided by $\beta(e^\beta - e^{-\beta})$. Then the intermediate value is multiplied by $e^\beta - e^{-\beta}$ and integrated in a loop. It is important to emphasize that though *NJOY* requires the first point of phonon DOS to be (*0*, *0*), this point is never used by the program. The first point of phonon DOS is instead prepared by applying the Debye parabolic

model using the second point. Therefore, in order to achieve comparable results with *NJOY*, our program follows this convention of *NJOY*. The next step is to calculate the crystallographic structure factor $f_i$ in corresponding reciprocal space position $\tau_i$. The structural factor defined in *NJOY* is

$$f_i = \frac{\pi^2 \hbar^2}{2 m_n N V} \sum_{\tau_i} \left| F(\boldsymbol{\tau}) \right|^2, \tag{3.4}$$

where $N$ is the number of atoms in the unit cell, $m_n$ is the mass of neutron, $V$ is the volume of the unit cell. The sum extends over all reciprocal lattice vectors of the given length $\tau_i$. The absolute square is given by

$$\left| F(\boldsymbol{\tau}) \right|^2 = \left| \sum_{j=1}^{N} \sqrt{\sigma_j} e^{i \boldsymbol{\tau} \cdot \mathbf{r}_j} \right|^2. \tag{3.5}$$

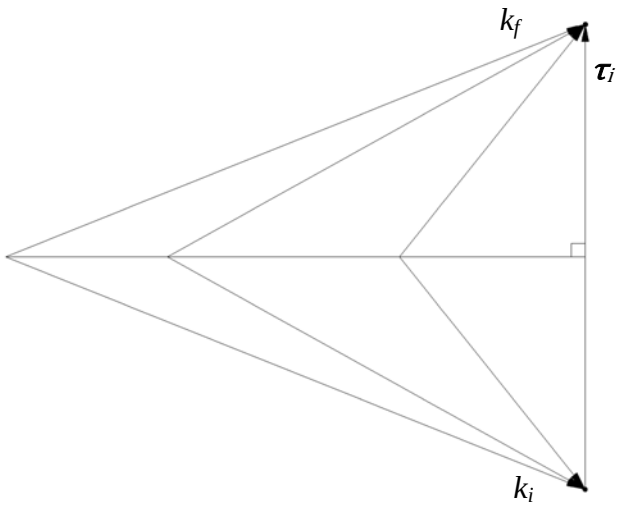


**Fig. 6. The elastic scattering in reciprocal space.**

Then the coherent elastic scattering cross section can be easily calculated with

$$\sigma_{coh}(E,\mu)=\frac{1}{E}\sum_{E_i<E}\frac{f_i}{\tau_i}e^{-4wE_i}\delta(\mu-\mu_i), \tag{3.6}$$

where the $\mu$ indicates cosine of scattering angle $\theta$, $\mu=\cos(\theta)$. The δ-function is the Bragg condition. $E_i$ are the so-called "*Bragg Edges*", and

$$\mu_i=1-E_i/E\,. \tag{3.7}$$

The Bragg Edge energy $E_i$ is defined as the smallest energy for a neutron to elastically scattered by a corresponding reciprocal space vector of magnitude $\tau_i$. As shown in Fig. 6, the smallest neutron energy can be obtained when $k_i$ is the smallest of all possible cases, that is, the case of backscattering: $k_i = \tau_i/2$. Therefore, $E_i$ is given by

$$E_i=\frac{\hbar^2 k_i^{\,2}}{2m_n}=\frac{\hbar^2\tau_i^{\,2}}{8m_n}. \tag{3.8}$$

### 3.1.2 Exact Coherent Elastic Scattering Cross Section

Instead of applying cubic approximation, there is no uniform Debye-Waller factor in this section. When the Debye-Waller factor is calculated in the exact way, the cross section can be applied to single crystal and inhomogeneous materials. The tradeoff for this generality is that the Debye-Waller factor now is different for every reciprocal lattice point $\boldsymbol{\tau}$. Correspondingly, the cross section $\sigma(\boldsymbol{\tau})$ should be a function of each reciprocal lattice point position. For example, if there are $50^3$=125,000 reciprocal lattice points, the Debye-Waller factor and the cross section have to be calculated for 125,000 times at each reciprocal space position $\boldsymbol{\tau}$. Then summation should be made of the cross section with the same $|\boldsymbol{\tau}|$.

As shown from Eq. (2.40) to Eq. (2.43), the Debye-Waller factor can be calculated from matrix $B_{ij}(\mu)$ which is integral of the partial phonon DOS and the off-diagonal DOS. In this work, the matrix $B_{ij}(\mu)$ is directly output by the software *PHONON 5.1.2* [26, 27] in the output file "*.d33". The reciprocal space vector $\boldsymbol{\tau} = h\mathbf{b}_1 + k\mathbf{b}_2 + l\mathbf{b}_3$ is achieved by the following steps.

First, the real space unit cell matrix **A** is read directly from input with the following format

$$\mathbf{A} = \begin{bmatrix} \mathbf{a}_1 & \mathbf{a}_2 & \mathbf{a}_3 \end{bmatrix} = \begin{bmatrix} a_{1x} & a_{2x} & a_{3x} \\ a_{1y} & a_{2y} & a_{3y} \\ a_{1z} & a_{2z} & a_{3z} \end{bmatrix}. \tag{3.9}$$

Then, the reciprocal space matrix **B** should have the relation with **A**: $\mathbf{B}=\mathbf{A}^{-1}$

$$\mathbf{B} = \begin{bmatrix} \mathbf{b}_1 \\ \mathbf{b}_2 \\ \mathbf{b}_3 \end{bmatrix} = \begin{bmatrix} b_{1x} & b_{1y} & b_{1z} \\ b_{2x} & b_{2y} & b_{2z} \\ b_{3x} & b_{3y} & b_{3z} \end{bmatrix}. \tag{3.10}$$

Next, $\boldsymbol{\tau}$ is

$$\boldsymbol{\tau} = \begin{bmatrix} h & k & l \end{bmatrix} \begin{bmatrix} \mathbf{b}_1 \\ \mathbf{b}_2 \\ \mathbf{b}_3 \end{bmatrix} = \begin{bmatrix} h & k & l \end{bmatrix} \begin{bmatrix} b_{1x} & b_{1y} & b_{1z} \\ b_{2x} & b_{2y} & b_{2z} \\ b_{3x} & b_{3y} & b_{3z} \end{bmatrix}. \tag{3.11}$$

Following by the calculation of $\boldsymbol{\tau}$, calculation of the Debye-Waller coefficient $W_\mu(\boldsymbol{\tau})$ can then be carried out for each $\boldsymbol{\tau}$ by applying Eq. (2.43). After point specified Debye-Waller coefficients for each atom type are obtained, $W_\mu(\boldsymbol{\tau})$ should be weighted over all types of atoms using Eq. (3.12) to acquire the Debye-Waller factor $w(\boldsymbol{\tau})$ for the material:

$$w(\boldsymbol{\tau}) = \sum_{\mu} W_{\mu}(\boldsymbol{\tau}) \frac{n_{\mu}}{n_{tot}}. \tag{3.12}$$

Finally Eq. (3.13) can be applied to calculate the cross section $\sigma(\boldsymbol{\tau})$ for each reciprocal point $\boldsymbol{\tau}$ utilizing $w(\boldsymbol{\tau})$

$$\sigma_{coh}\left(\boldsymbol{\tau}, E, \mu\right) = \frac{1}{E} \sum_{E_i < E} \frac{f_i}{\left|\boldsymbol{\tau}\right|} e^{-4w(\boldsymbol{\tau})E_i} \delta\left(\mu - \mu_i\right), \tag{3.13}$$

in which, the magnitude of $|\boldsymbol{\tau}|$ can also be easily obtained by

$$\begin{aligned} \left|\boldsymbol{\tau}\right|^2 = \frac{1}{V^2}[&h^2b^2c^2\sin^2\alpha + k^2a^2c^2\sin^2\beta + l^2a^2b^2\sin^2\gamma + \\ &2hkabc^2F\left(\alpha,\beta,\gamma\right) + 2kla^2bcF(\beta,\gamma,\alpha) + 2lhab^2cF(\gamma,\alpha,\beta)] \end{aligned}, \tag{3.14}$$

where

$$F(\alpha,\beta,\gamma) = \cos\alpha\cos\beta - \cos\gamma, \tag{3.15}$$

$V$ is the volume of the unit cell,

$$V^2 = a^2b^2c^2(1 - \cos^2\alpha - \cos^2\beta - \cos^2\gamma + 2\cos\alpha\cos\beta\cos\gamma). \tag{3.16}$$

{$a$, $b$, $c$, $\alpha$, $\beta$, $\gamma$} is the standard crystallographic notation of a crystal unit cell [28]. The reciprocal space dependent cross section $\sigma_{coh}\left(\boldsymbol{\tau}, E, \mu\right)$ can then be summed over each $\boldsymbol{\tau}$ with the same magnitude to obtain the energy dependent cross section $\sigma_{coh}\left(E, \mu\right)$.

Up to this point, calculation strategy of the coherent elastic cross section is well established. One last point that should be pointed out is that the cross section shall be output directly by a standalone program developed by this work. However, only after implemented into *LEAPR* module in *NJOY*, useful cross section data file in ENDF/B-VII format can be obtained. Though following the convention of *NJOY*, the *LEAPR* module outputs $E\sigma(E)$

instead of $\sigma(E)$, $E\sigma(E)$ is divided by $E$ in the *THERMER* module. Therefore, the output passing through *THERMER* module shall be the cross section instead of the cross section multiplied by the energy.

## 3.2 Computation of Inelastic Scattering Cross Section

The inelastic cross section under incoherent approximation can be simplified to the following form using unitless momentum transfer $\alpha$ and energy transfer $\beta$,

$$\left(\frac{d^2\sigma}{d\Omega dE'}\right)_{inel} = \frac{\sigma}{4\pi k_B T}\sqrt{\frac{E'}{E}}\sum_{n>0} {}^{n}S_s(\alpha,\beta), \tag{3.17}$$

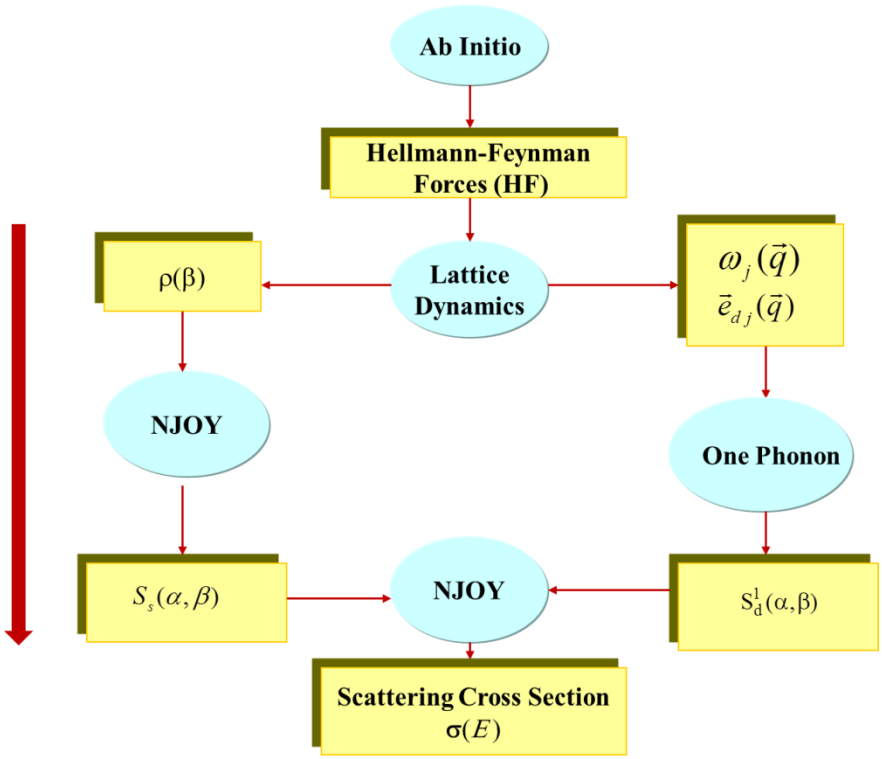


**Fig. 7. Calculation flow chart for inelastic cross section.**

As shown in Fig. 7 the left hand side is the incoherent inelastic routine while the right hand side is the coherent one-phonon routine. In this work, only the incoherent inelastic routine will be adopted because in 3C-SiC, the coherent inelastic cross section is in orders of magnitude smaller than incoherent inelastic cross section. After phonon DOS $\rho(\beta)$ is obtained from lattice dynamics program, calculations of the scattering law $S_s(\alpha,\beta)$ and the cross section are handled by *LEAPR* module in *NJOY*. The scattering law $S_s(\alpha,\beta)$ uses a 100×100 ($\alpha$, $\beta$) mesh. Calculation of $S_s(\alpha,\beta)$ proceed with phonon expansion to the order of 100. All calculation is set under room temperature 300 *K*.

An *Ab Initio* program named *VASP* [29-32] is used with combination of lattice dynamics program *PHONON* 5.1.2 to generate the phonon DOS. Lattice dynamics method is an important predictive method commonly used to calculate phonon frequencies $\omega(\boldsymbol{\tau})$ in reciprocal lattice point [33]. The eigenvalues of the dynamical matrix $\mathbf{D}(\boldsymbol{\tau})$ give the squares of allowed phonon frequencies $\omega(\boldsymbol{\tau})^2$ for a given reciprocal point $\boldsymbol{\tau}$ in first Brillouin zone. Therefore, the more points that are sampled in reciprocal space the more accurate the phonon DOS will be. The dynamical matrix $\mathbf{D}(\boldsymbol{\tau})$ is a 3×3 matrix generated from secondary partial derivative of crystal potential to atom displacement. The potential and forces in the crystal, therefore, need to be defined beforehand in order to fulfill the goal of generating dynamical matrix. There are generally two routines that can be followed nowadays to generate interatomic forces.

The conventional classical method extracts atomic forces from fitting experiment data. This method, however, might bring in unnecessary uncertainty from experiment. It also renders huge percentage of variation in the low frequency range of phonon DOS, which has a

huge impact on the scattering law and scattering cross section. In this research, the a*b-initio* methods are deployed to provide atomic potential and analyze the forces. Program *VASP* is chosen because it exhibits the best agreement with interatomic potential according to our experience.

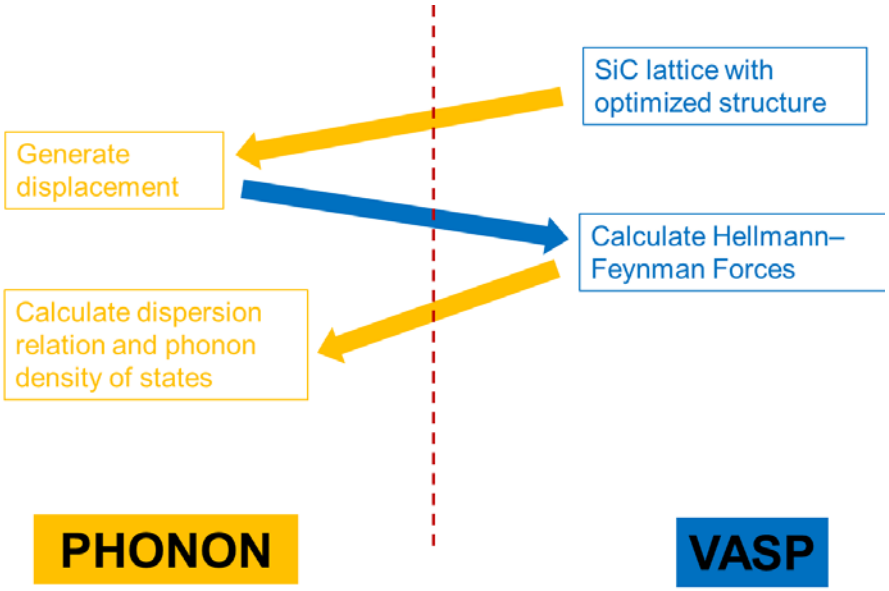


**Fig. 8. Flow chart of generating phonon DOS.**

Figure 8 demonstrates a flow chart of how the phonon DOS is fulfilled by utilizing *PHONON* and *VASP*. A 3C-SiC unit cell with the lattice parameter $a$=4.395 *Å* is first built in *VASP*. Then atoms in the unit cell are relaxed to their equilibrium position with the lattice parameter minimized to its lowest energy. The electronic structure calculation utilized the generated gradient approximation (GGA) with a plane wave cut off energy of 900 eV. A 3×3×3 Monkhorst-Pack k-mesh and tetrahedron smearing scheme were used to for integration. The convergence of energy is set to be $1\times10^{-5}$ *eV*. Thus a minimized 3C-SiC

unit cell with *a=4.379 Å* at 0 *K* is built. The minimized unit cell is then put into *PHONON* to generate a 3×3×3 supercell with 216 atoms in it. Because the unit cell holds only 2 non-equivalent atoms at high symmetry positions, a total of 4 displacements are sufficient enough to construct the dynamical matrix. One of the carbon atoms is displaced by ±0.02 *Å* and another silicon atom is displaced by ±0.02 *Å*. Four position cards with displaced atom position are then generated by phonon program. These position cards are put into *VASP* using *VASP*'s pseudopotential to calculate the Hellmann-Feynman forces of each displaced system. These outputs from *VASP* are again input into *PHONON* which yields dynamical matrix. With the dynamical matrix generated, Monte-Carlo sampling in the first Brillouin zone can be carried out to produce phonon dispersion curve as wells as phonon DOS. When generating phonon dispersion curve, *LO-TO* splitting is applied to split longitudinal optical and transverse optical dispersion curves. In this research, the phonon DOS is sampled with 1 million points and sorted into *0.001 eV* energy bars.

# Chapter 4 Results

This study proposed the theory and strategy to calculate the cross section of polycrystalline materials. Based on the derivation of Eq. (3.6), a complete routine of calculating coherent elastic cross section is developed. In order to generate necessary information to calculate Debye-Waller factor, phonon DOS is extrapolated from VASP and PHONON. Both inelastic and coherent elastic cross sections are processed by NJOY code system and available as ENDF/B-VII library.

## 4.1 Development of New Coherent Elastic Routine in *LEAPR/NJOY*

The new coherent elastic routine is completely rewritten and is more sophisticated and versatile than the original NJOY routine. Comparison of the new routine and the old one is made in Table 2.

Table 2. Comparison of old routine and updated routine.

| | Old routine | New routine |
|---|---|---|
| Supported structure | Hexagonal, FCC, BCC | Any crystal structure |
| Supported material | Graphite, beryllium, beryllium oxide, aluminum, lead, iron | Any material |
| Debye-Waller Factor | Approximated | Exact |
| Need to modify source code if calculating other materials | Yes | No |

There are two basic routines you can choose to accomplish the coherent elastic cross section calculation. One is the cubic approximation routine. Another is the single crystal routine. The cubic approximation, in general, applies to any polycrystalline structure. Even

for non-cubic crystal the approximation is often close enough that the algorithm is still correct. In case of a non-isotropic crystal, where there is an orientation preference in a particular direction throughout the whole crystal, the second "exact Debye-Waller Factor" routine is recommended to calculate the coherent elastic cross section. In the input card of *NJOY*, the 4th entry of card 5 of *LEAPR* input card controls the coherent elastic routine (see Table 3 below). It should be specified in *NJOY* input card which coherent elastic routine to execute.

Table 3. Input card 5 for *LEAPR/NJOY*.

| | |
|---|---|
| * card 5 - principal scatterer control | * |
| * awr weight ratio to neutron for principal scatterer | * |
| * spr free atom cross section for principal scatterer | * |
| * npr number of principal scattering atoms in compound | * |
| * iel coherent elastic option | * |
| * 0 none (default) | * |
| * 1 cubic approximation | * |
| * 2 exact Debye-Waller Factor | * |
| * ncold cold hydrogen option | * |
| * 0 none (default) | * |
| * 1 ortho hydrogen | * |
| * 2 para hydrogen | * |
| * 3 otho deuterium | * |
| * 4 para deuterium | * |
| * nsk 0 none (default) | * |
| * 1 vinyard | * |
| * 2 skold | * |

Despite the NJOY's original input card, there is an independent input card you need to prepare for the new coherent elastic routine. It should be named "coh_input"; otherwise it will not be recognized by the program. Depending on the approximation you choose in the program, the input card varies. The input card contains important information regarding

structure parameters, bound cross sections and dynamic force information.

## 4.2 Phonon Properties for 3C-SiC

Though the phonon DOS $\rho(\omega)$, a property directly determines inelastic scattering cross section, cannot be benchmarked due to lack of current experiment data, the phonon dispersion curve can be compared to current existing experiment to prove the trustiness of our calculation. Figure 9 shows a comparison of phonon dispersion curve with experiment data [1, 2].

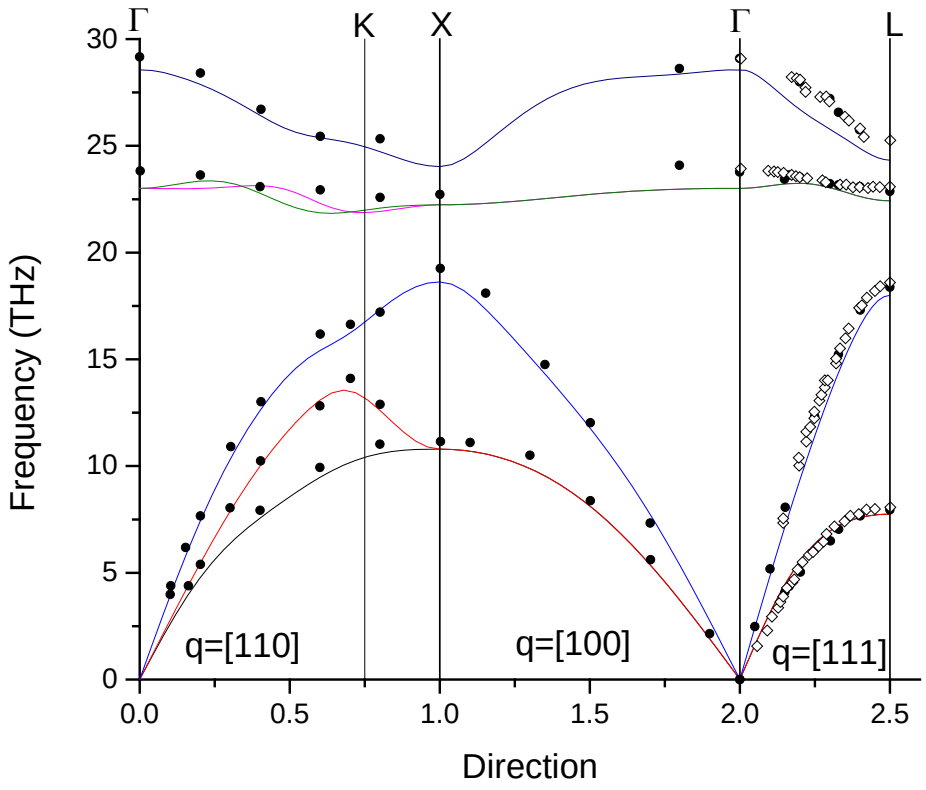


**Fig. 9. Phonon dispersion curve compared to experimental data from Ref. [1, 2].**

It is important to point out that the frequency output from *PHONON* in Fig. 9 is not the angular frequency $\omega$ in Eq. (2.36), but rather $\nu$, where $\nu$ and $\omega$ are related by $\omega = \nu \cdot 2\pi$. As $k$ approaches zero (the long-wavelength limit), acoustic branches of phonon dispersion curve exhibit linear response to its frequency. The parabolic potential from *VASP* which assumes force is proportional to displacement gives rise to this linear response between $\omega$ and $k$. It gives rise to the parabolic shape in low frequency region of phonon DOS. This is due to the fact that in the very low frequency range the DOS is proportional to square of frequency multiplied by group velocity, which is the derivative of $\omega$ to $k$

$$\rho(\omega) \propto \omega^2 \frac{\partial \omega}{\partial k}, \omega \ll 1. \tag{4.1}$$

When linearity between $\omega$ and $k$ renders the partial derivative a constant in Eq. (4.1), the phonon DOS becomes proportional to $\omega^2$. Figure 10 illustrates phonon DOS of 3C-SiC from 1,000,000 sampling points in k-space and then distributed into $1\times10^{-3}$ *eV* interval energy bars. As shown in the DOS, low energy region DOS is primarily contributed by Si atoms while high energy region DOS is mainly contributed by C atoms. Since C is lighter than Si, it is easier for C to vibrate with higher frequency under the same magnitude of force. Therefore, the acoustic branches of phonon dispersion curve are mainly results of Si atoms vibration while the optical branches mainly stems from C atoms. It should be noted that though the Debye temperature of 3C-SiC is 1200 *K*, which corresponds to 0.1 *eV*, the parabolic region ends much earlier around 0.03 *eV*. Thus, the Debye model is applied in this research with the phonon DOS fitted into a parabolic curve only in the energy range 0 *eV* ~ 0.02 *eV*.

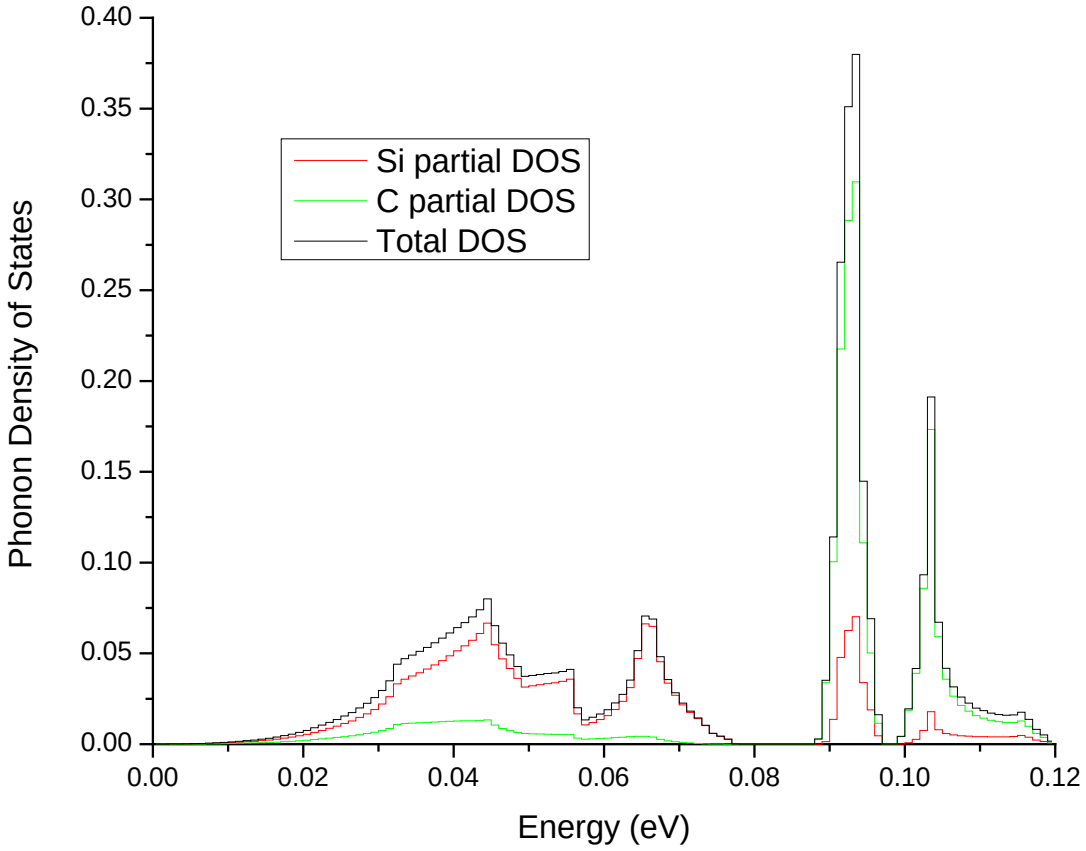


**Fig. 10. Phonon density of states for 3C-SiC.**

## 4.3 Inelastic Scattering Cross Section for 3C-SiC

There are many necessary steps in obtaining the inelastic scattering cross section. The first is to calculate the partial DOS of Si and C atoms as shown in the previous section. The second step is to subtract scattering law from incoherent approximation and Gaussian approximation. The scattering law is calculated from a Fourier transform in *LEAPR* module and is partly shown in Fig. 11.

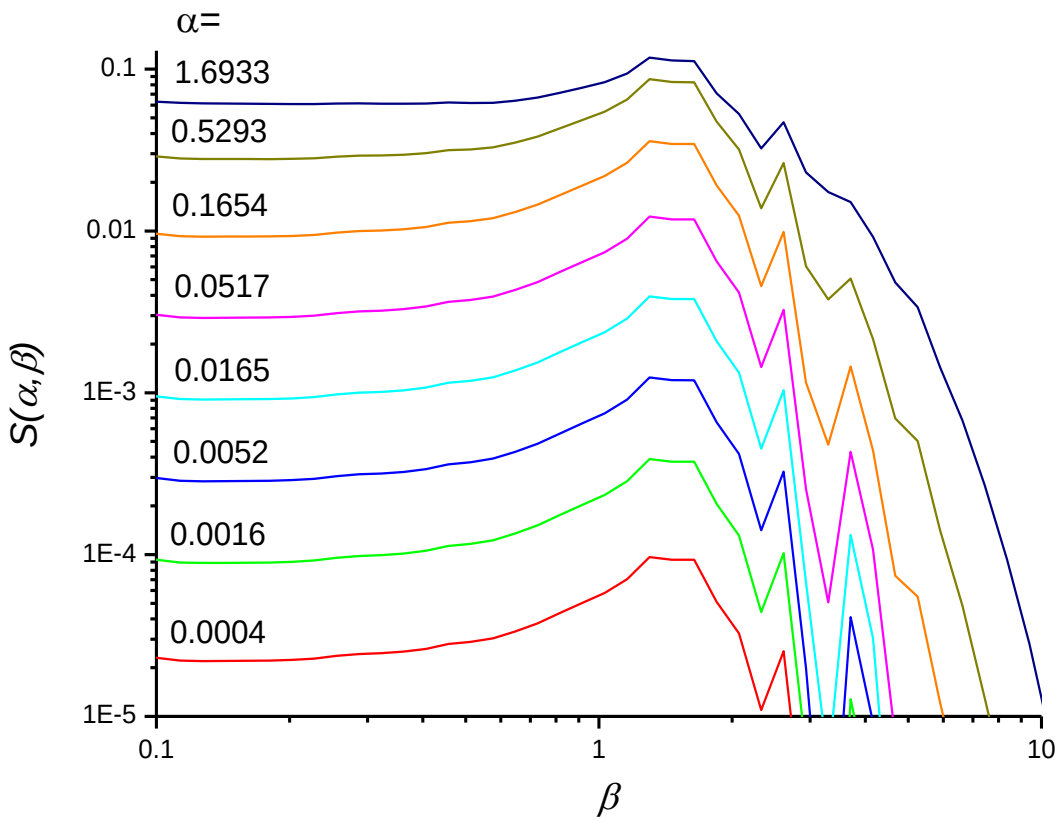


**Fig. 11. Scattering law of 3C-SiC *vs.* $\beta$ for various $\alpha$.**

The inelastic cross section is then directly obtained by the following equation

$$\sigma\left(E \to E', \mu\right) = \frac{\sigma_b}{2k_B T}\sqrt{\frac{E'}{E}}S(\alpha,\beta)\,. \tag{4.2}$$

Equation (4.2) shows that the cross section is basically product of three independent variables and is proportional to the scattering law $S(\alpha,\beta)$. The first variable is $\sigma_b$, i.e., bound cross section of neutron, gives the information of the interaction between neutrons and scattering material. The second variable $\sqrt{E'/E}$ depends on the change of energy of neutron during the scattering process. The third factor, scattering law $S(\alpha,\beta)$, is independent on neutron property,

that is, neither its intrinsic property nor its interaction with scattering system. The only attribution to the scattering law is the scattering system, i.e., its atom vibration mode, forces between atoms, phonon distribution and crystal lattice structure. Therefore, $S(\alpha,\beta)$ is a separated factor that contributes to inelastic cross section from scattering system.

Secondary scattering cross sections can then be evaluated by Eq. (4.2). The secondary neutron spectra are partly shown in Fig. 12. They are integrals of double differential cross sections over all possible scattering directions.

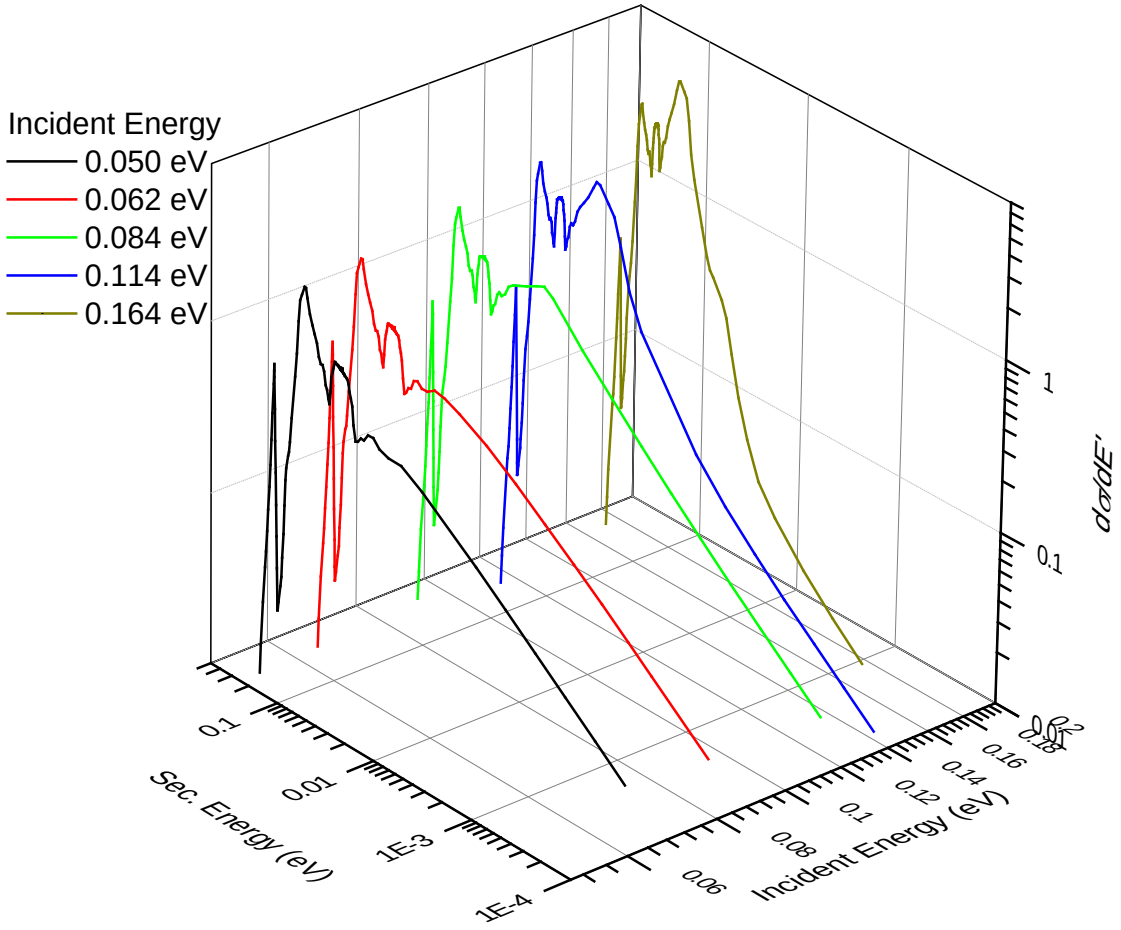


**Fig. 12. Secondary neutron spectra of C atoms in 3C-SiC.**

In Fig. 12 an incident neutron energy range just above the thermal neutron energy is selected to show the up-scatter and thermalization behavior. It can be seen that the down-scattering peak is flattened out to lower energy region when incident neutron energy decreases. The thermalization behavior is directly exhibited by the fact that integral over down-scattering peak is larger than that of up-scattering peak. By integrating every secondary spectrum over scattered neutron energies *E′*, a total scattering cross section for each atom type can be obtained. The total cross section for C and Si and SiC is plotted in Fig. 13.

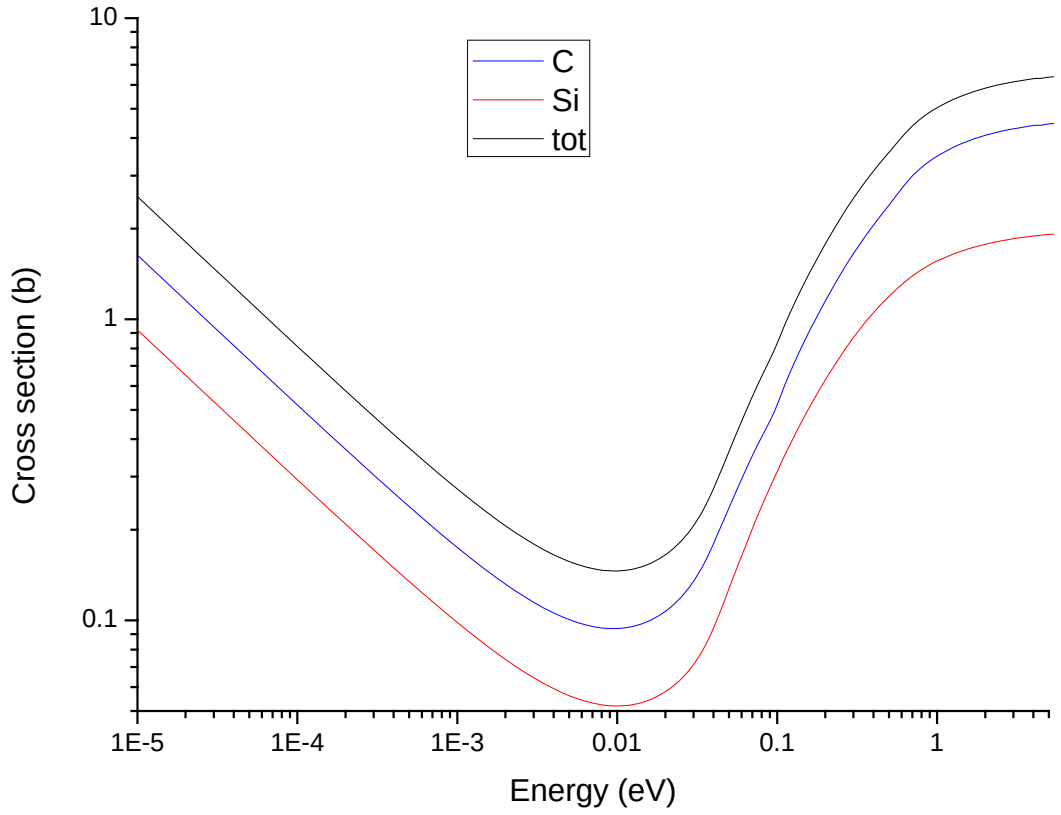


**Fig. 13. Inelastic cross section for 3C-SiC unit cell.**

The inelastic cross section shown in Fig. 13 is the one averaged per atom pair. In another word, the cross section is averaged over all four pairs of Si and C atoms in the unit cell. As shown in the plot, a minimum inelastic cross section can be found around 0.01 *eV*. Thermal neutrons around 0.01 *eV* will therefore have minimum probability of inelastic scattering with silicon carbide. This "transparency" to thermal neutrons renders 3C-SiC capability to be a promising nuclear structural and fuel material candidate.

## 4.4 Coherent Elastic Scattering Cross Section for 3-C SiC

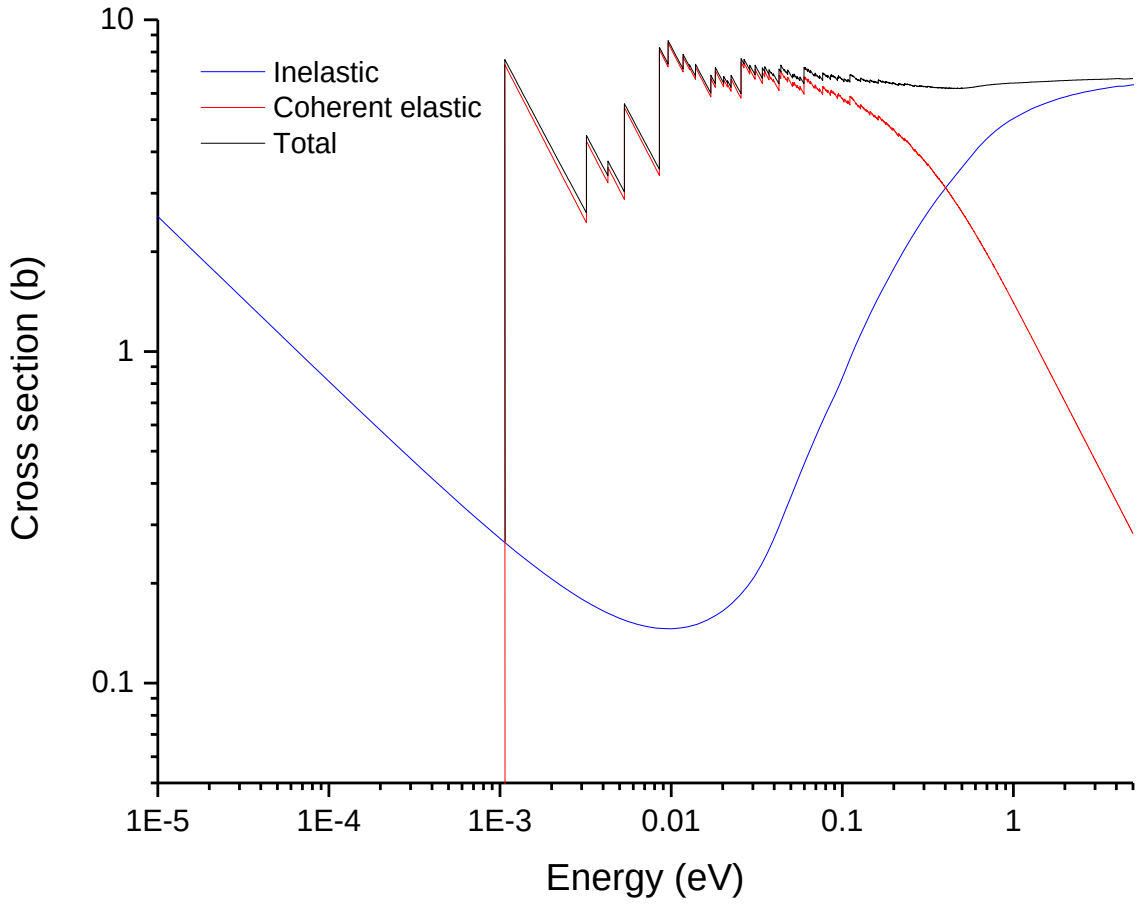


**Fig. 14. Coherent elastic cross section of 3C-SiC.**

The coherent elastic scattering cross section for a polycrystalline 3C-SiC is illustrated in Fig. 14 together with the inelastic cross section. Unlike the inelastic cross section, which is extrapolated from partial DOS of Si and C atoms, the coherent elastic cross section is calculated by Eq. (3.1) using total phonon DOS. Both the coherent elastic and inelastic cross sections are prepared in *ENDF/B-VII* libraries (Please refer to Appendix C).

The manner in which neutrons scattered by polycrystalline material can be explained by Eq. (3.6). As shown by Fig. 6 and Eq. (1.2), maximum momentum change occurs in the situation of back scattering. Hence, when wave vector is less than one half of the smallest $\tau_i$, coherent elastic scattering could not happen. The first coherent elastic scattering occurs when energy increases till the wave length of a neutron equals to two times of the maximum of plane spacing in the lattice: $\lambda=2d_{max}$ (equivalent to $2\boldsymbol{k}_i=\tau_{min}$). In this situation, the incident neutron wave direction $\boldsymbol{k}_i$ is perpendicular to the plane with spacing $d_{max}$. At slightly higher energy, the cross section results from planes with spacing $d_{max}$ decrease with increasing $k_i$, being proportional to *1/E*. As the incident energy increases to the second Bragg edge, the cross section jumps to another maximum value as it is a summation of all contributions of suitable reflection planes in Eq. (3.6). As energy further increases to several *eV*, cross section appears as a visually smooth curve decreasing with *E*. This is because there are so many planes contributing to the summation in Eq. (3.6) and they are all very small due to damping from the Debye-Waller factor. As energy approaches several *eV*, the coherent elastic cross section becomes very small. The total cross section remains near free atom cross section due to the compensation from the increase in inelastic cross section. When the neutron energy is large enough, neutron scattering is essentially the same from that by free

atoms at rest because the phonon energy is negligible compared to the neutron energy. Thus, phonons can hardly make any significant contribution to the cross section.

# Chapter 5 Conclusion and Future Work

In this work, computational analysis of thermal neutron scattering in 3C-SiC was performed. Starting from the basic definition of the cross section, two basic assumptions are made to deduce an expression for the cross section. The first one is the Born approximation from first order time perturbation theory. The second is Fermi's pseudopotential which assumes that the scattering potential is a δ-function. Based upon these assumptions, quantum mechanics is utilized to mathematically quantify cross section in the form of scattering law.

Approximations and assumptions are needed to transform the theory to a programmable equation. The first is the harmonic approximation, which assumes that the forces in crystal lattice are proportional to displacements. This approximation allows us to use phonon theory and expand scattering as shown in Eq. (2.16) and Eq. (2.17). The second is the cubic approximation, which assumes that the sample takes the form of a polycrystalline material. This approximation is in fact accurate for polycrystalline materials. The third approximation is that there exists a single universal Debye-Waller factor that can be applied to every atom in the sample and generate correct averaged cross sections. This approximation generally averages out the effect of the different scattering length of each atom and the orientation preferred micro-crystalline arrangement.

With these assumptions and approximations applied, the phonon properties of 3C-SiC are calculated and presented as dispersion relations and phonon density of states (DOS). The phonon dispersion curves show consistent agreement with existing experimental data, which ensures the correctness of our partial phonon DOS of C and Si atoms in 3C-SiC. The phonon properties are then implemented into the NJOY program to calculate the cross sections as

well as generate the ENDF standard libraries. Modifications and explanations of *LEAPR/NJOY* module are made to make the code more flexible and general. A more versatile standalone code that is capable of calculating the cross sections for both single crystal and polycrystalline materials is developed. Though 3C-SiC is the focus of the present work, the newly developed routine in *LEAPR/NJOY* is applicable to all polycrystalline materials.

Due to the lack of experimental thermal scattering cross section data for 3C-SiC, the current work can benefit from performing measurements. Experiments for measuring the total cross section are currently being considered at the *NCSU PULSTAR* reactor.

## REFERENCES


[1] S. Bagci, S. Duman, H.M. Tutuncu, G.P. Srivastava, "Theoretical studies of SiC, AlN and their (110) surfaces", DIAM. RELAT. MAT. **18**, 1057 (2009).

[2] K. Karch, P. Pavone, W. Windl, D. Strauch, F. Bechstedt, "Ab initio calculation of structural, lattice dynamical, and thermal properties of cubic silicon carbide", INTERNATIONAL JOURNAL OF QUANTUM CHEMISTRY. **56**, 801 (1995).

[3] R. Jones, L. Snead, A. Kohyama, P. Fenici, "Recent advances in the development of SiC/SiC as a fusion structural material", FUSION ENG. DES. **41**, 15 (1998).

[4] N.R. Brown, H. Ludewig, A. Aronson, G. Raitses, M. Todosow, "Neutronic evaluation of a PWR with fully ceramic microencapsulated fuel. Part I: Lattice benchmarking, cycle length, and reactivity coefficients", ANN. NUCL. ENERGY. **62**, 538 (2013).

[5] K.A. Terrani, J.O. Kiggans, Y. Katoh, K. Shimoda, F.C. Montgomery, B.L. Armstrong, C.M. Parish, T. Hinoki, J.D. Hunn, L.L. Snead, "Fabrication and characterization of fully ceramic microencapsulated fuels", J. NUCL. MATER. **426**, 268 (2012).

[6] L.L. Snead, T. Nozawa, Y. Katoh, T. Byun, S. Kondo, D.A. Petti, "Handbook of SiC properties for fuel performance modeling", J. NUCL. MATER. 371, 329 (2007).

[7] L. Charpentier, M. Balat-Pichelin, H. Glénat, E. Bêche, E. Laborde, F. Audubert, "High temperature oxidation of SiC under helium with low-pressure oxygen. Part 2: CVD β-SiC", JOURNAL OF THE EUROPEAN CERAMIC SOCIETY. **30**, 2661 (2010).

[8] L. Charpentier, M. Balat-Pichelin, F. Audubert, "High temperature oxidation of SiC under helium with low-pressure oxygen—Part 1: Sintered α-SiC", JOURNAL OF THE EUROPEAN CERAMIC SOCIETY. **30**, 2653 (2010).

[9] J. Selvakumar, D. Sathiyamoorthy, "Prospects of chemical vapor grown silicon carbide thin films using halogen-free single sources in nuclear reactor applications: A review", J. MATER. RES. **28**, 136 (2012).

[10] S. Sharafat, R.H. Jones, A. Kohyama, P. Fenici, "Status and prospects for SiC/SiC composite materials development for fusion applications", FUSION ENG. DES. **29**, 411 (1995).

[11] A. Owens, A. Peacock, "Compound semiconductor radiation detectors", NUCLEAR INSTRUMENTS AND METHODS IN PHYSICS RESEARCH SECTION A: ACCELERATORS, SPECTROMETERS, DETECTORS AND ASSOCIATED EQUIPMENT. **531**, 18 (2004).

[12] F.H. Ruddy, A.R. Dulloo, J.G. Seidel, S. Seshadri, L.B. Rowland, "Development of a silicon carbide radiation detector", NUCLEAR SCIENCE, IEEE TRANSACTIONS ON. **45**, 536 (1998).

[13] J.B. Casady, R.W. Johnson, "Status of silicon carbide (SiC) as a wide-bandgap semiconductor for high-temperature applications: A review", SOLID-STATE ELECTRONICS. **39**, 1409 (1996).

[14] H. Matsunami, T. Kimoto, "Step-controlled epitaxial growth of SiC: High quality homoepitaxy", MATERIALS SCIENCE AND ENGINEERING: REPORTS. **20**, 125(1997).

[15] Y. Xu, L. Cheng, L. Zhang, "Carbon/silicon carbide composites prepared by chemical vapor infiltration combined with silicon melt infiltration", CARBON. **37**, 1179 (1999).

[16] C.A. Zorman, R.J. Parro, "Micro- and nanomechanical structures for silicon carbide MEMS and NEMS". STATUS SOLIDI B-BASIC SOLID STATE PHYS. **245**, 1404 (2008).

[17] J.P. de Villiers, J. Roberts, N. Ngoepe, A.S. Tuling, "Evaluation of the Phase Composition, Crystallinity, and Trace Isotope Variation of SiC in Experimental TRISO Coated Particles", JOURNAL OF ENGINEERING FOR GAS TURBINES AND POWER. 131 (2009).

[18] Z. Dauter, M. Jaskolski, "How to read (and understand) Volume A of International Tables for Crystallography: an introduction for nonspecialists", J. APPL. CRYSTALLOGR. **43**, 1150 (2010).

[19] J.K. Shultis, R.E. Faw, "Fundamentals of nuclear science and engineering", MARCEL DEKKER NEW YORK, 2002.

[20] G.L. Squires, "Introduction to the theory of thermal neutron scattering", CAMBRIDGE UNIVERSITY PRESS, 2012.

[21] A.I. Hawari, I. Al-Qasir, V.H. Gillette, B.W. Wehring, T. Zhou, "Ab initio generation of thermal neutron scattering cross sections", PHYSOR 2004: THE PHYSICS OF FUEL CYCLES AND ADVANCED NUCLEAR SYSTEMS - GLOBAL DEVELOPMENTS, 551 (2004).

[22] A.I. Hawari, I. Al-Qasir, "Graphite thermal neutron scattering cross section calculations including coherent 1-phonon effects". PHYSOR 2008: INTERNATIONAL CONFERENCE ON THE PHYSICS OF REACTORS 2008, **1**, 347 (2008).

[23] E. Amaldi, "The production and slowing down of neutrons, in: Neutrons and Related Gamma Ray Problems", SPRINGER, 1959.

[24] R. Macfarlane, R. Boicourt, "NJOY - Neutron and Photon Cross-Section Processing System", TRANSACTIONS OF THE AMERICAN NUCLEAR SOCIETY. **22**, 720 (1975).

[25] R.E. MacFarlane, A.C. Kahler, "Methods for Processing ENDF/B-VII with NJOY", NUCL. DATA SHEETS. **111**, 2739 (2010).

[26] K. Parlinski, Z. Li, Y. Kawazoe, "First-principles determination of the soft mode in cubic ZrO2", PHYS. REV. LETT. **78**, 4063 (1997).

[27] K. Parlinski, "Software Phonon", CRACOW (2010).

[28] M. De Graef, M.E. McHenry, "Structure of materials: an introduction to crystallography, diffraction and symmetry", CAMBRIDGE UNIVERSITY PRESS, 2007.

[29] G. Kresse, J. Hafner, "Ab initio molecular dynamics for liquid metals, PHYSICAL REVIEW B". **47**, 558 (1993).

[30] G. Kresse, J. Hafner, "Ab initio molecular-dynamics simulation of the liquid-metal–amorphous-semiconductor transition in germanium", PHYSICAL REVIEW B. **49**, 14251 (1994).

[31] G. Kresse, J. Furthmüller, "Efficiency of ab-initio total energy calculations for metals and semiconductors using a plane-wave basis set", COMPUTATIONAL MATERIALS SCIENCE. **6**, 15 (1996).

[32] G. Kresse, J. Furthmüller, "Efficient iterative schemes for ab initio total-energy calculations using a plane-wave basis set", PHYSICAL REVIEW B. **54**, 11169 (1996).

[33] A.A. Maradudin, E.W. Montroll, G.H. Weiss, I. Ipatova, "Theory of lattice dynamics in the harmonic approximation", ACADEMIC PRESS NEW YORK, 1963.

# APPENDICES

## Appendix A Comprehending the Coherent Elastic Scattering Formula

Equation (1.5) gives the form of neutron waves scattered from one atom fixed at origin. However, in a scattering experiment, a beam of neutrons is scattered by a set of atoms in a sample. In the situation of multi-atom scattering, each atom, labeled by index *j*, will make a contribution to the scattered wave. When an atom is located at $\boldsymbol{R}_j$, the scattered wave contributed by this atom would be

$$\psi_{f,j} = -\psi_0 e^{i\mathbf{k_i}\cdot\mathbf{R_j}} b_j \frac{e^{i\mathbf{k_f}\cdot(\mathbf{r}-\mathbf{R_j})}}{\left|\mathbf{r}-\mathbf{R_j}\right|} = -\psi_0 e^{i\mathbf{k_f}\cdot\mathbf{r}} b_j \frac{e^{i\mathbf{Q}\cdot\mathbf{R_j}}}{\left|\mathbf{r}-\mathbf{R_j}\right|}. \tag{A.1}$$

For simplification purpose, it is assumed that the sample has only one atom per unit cell and the scattering length is a constant for all atoms. Under this assumption, the subscript *j* for $b_j$ can be dropped. In a neutron experiment, our detector is always far away enough from the sample to ignore the distance between atom positions. Then the denominator can be put as *r*. Eq. (A.1) is simplified as

$$\psi_{f,j} = -\frac{\psi_0 e^{i\mathbf{k_f}\cdot\mathbf{r}} b}{r} e^{i\mathbf{Q}\cdot\mathbf{R_j}}. \tag{A.2}$$

We will start from a two-atom sample to illustrate how the interference term in coherent elastic scattering cross section comes into place. The differential cross section is

$$\begin{aligned}\left(\frac{d\sigma}{d\Omega}\right)_{el} &= \frac{\iint \left|\psi_f\right|^2 dA}{\left|\psi_i\right|^2 d\Omega} \\ &= \frac{b^2}{2}\left|e^{i\mathbf{Q}\cdot\mathbf{R_1}} + e^{i\mathbf{Q}\cdot\mathbf{R_2}}\right|^2 \\ &= \frac{b^2}{2}\left[2 + 2\cos\left(\mathbf{Q}\cdot\left(\mathbf{R_1}-\mathbf{R_2}\right)\right)\right]\end{aligned}.$$

In the situation of three atoms,

$$\left(\frac{d\sigma}{d\Omega}\right)_{el} = \frac{b^2}{2}\left|e^{i\mathbf{Q}\cdot\mathbf{R}_1} + e^{i\mathbf{Q}\cdot\mathbf{R}_2} + e^{i\mathbf{Q}\cdot\mathbf{R}_3}\right|^2$$
$$= \frac{b^2}{3}\left[3 + 2\cos\left(\mathbf{Q}\cdot\left(\mathbf{R}_1 - \mathbf{R}_2\right)\right) + 2\cos\left(\mathbf{Q}\cdot\left(\mathbf{R}_1 - \mathbf{R}_3\right)\right) + 2\cos\left(\mathbf{Q}\cdot\left(\mathbf{R}_3 - \mathbf{R}_2\right)\right)\right].$$

As can be seen, the first constant combined with scattering length coefficient outside of bracket is Eq. (1.9). This term attributes scattering without interaction between atoms. The rest are cosine terms rising from interference of scattered wave from different atoms. When there are $N$ atoms in the sample located at $R_1 \ldots R_N$, elastic cross section is

$$\left(\frac{d\sigma}{d\Omega}\right)_{el} = \frac{b^2}{N}\left|\sum_{j=1}^{N} e^{i\mathbf{Q}\cdot\mathbf{R}_j}\right|^2. \tag{A.3}$$

It should be remarked that three assumptions are applied thus far. The first is that each atom is located at their position without thermal vibration. The second is that there is only one atom type with a constant scattering length in the sample, in which there is only one atom per unit cell (Bravais lattice). The third approximation should be very accurate, which is the far field approximation.

In the situation of a crystal structure, summation in Eq. (A.3) can be greatly simplified by the periodicity of a crystal lattice. Utilizing the same trick from Eq. (2.32) to (2.33), Eq. (A.3) is

$$\frac{d\sigma^{\tau}_{el,coh}(\mathbf{k_f})}{d\Omega} = \frac{(2\pi)^3}{v_0} b^2 \delta(\mathbf{Q} + \boldsymbol{\tau}). \tag{A.4}$$

An upper index $\boldsymbol{\tau}$ has been attached to the symbol of the differential cross section in (A.4) in order to recall that it represents the contribution arising from the reflection of planes of Miller indices ($h$,$k$,$l$). In a polycrystalline material, scattering with all directions of $\boldsymbol{\tau}$ is

equally possible. Equation (A.4) is, therefore, another version of Eq. (2.34) with the proposed approximation applied. Hence, expression (A.4) should be averaged over all direction of $\boldsymbol{\tau}$ in reciprocal space.

$$\begin{aligned}\left(\frac{d\sigma_{el,coh}^{\tau}}{d\Omega}\right)_{av} &= \frac{1}{4\pi}\int \frac{d\sigma_{el,coh}^{\tau}}{d\Omega}\sin\theta_{\tau}d\varphi_{\tau}d\theta_{\tau} \\ &= \frac{b^2}{2v_0\tau^2}\delta(2k_i\sin\theta-\tau)\end{aligned} \quad . \tag{A.5}$$

Equation (A.5) tells a scattering event with the magnitude of $\tau$, and scatter angle of $\theta$. In order to obtain the total scattering cross section regardless the direction of scattered neutron, Eq. (A.5) should be integrated over all directions of scattered neutron in real space.

$$\begin{aligned}\left(\sigma_{el,coh}^{\tau}\right)_{av} &= 2\pi\int\left(\frac{d\sigma_{el,coh}^{\tau}}{d\Omega}\right)_{av}\sin 2\theta d2\theta \\ &= \frac{b^2\lambda^2}{2v_0}\frac{1}{\tau}\end{aligned} \quad . \tag{A.6}$$

The total coherent elastic cross section is finally obtained by summing all the $\tau$

$$\sigma_{el,coh} = \frac{b^2\lambda^2}{2v_0}\sum_{\tau\le 2/\lambda}\frac{1}{\tau}. \tag{A.7}$$

When introducing multiple atoms into a unit cell, the structure factor should come into place in Eq. (A.7). Furthermore, by considering thermal vibration of atoms around their equilibrium position, Debye-Waller factor will be introduced. In conclusion,

$$\sigma_{el,coh} = \frac{\lambda^2}{2v_0}\sum_{\tau\le 2/\lambda}\frac{1}{\tau}\left|F(\boldsymbol{\kappa})\right|^2 \tag{A.8}$$

in which $F(\boldsymbol{\kappa})$ is shown in Eq. (2.35).

## Appendix B Comparison of Different Coherent Elastic Scattering Formula

In this appendix, it will be demonstrated that Eq. (2.34), (A.8) and (3.6) (listed as Eq. (B.1) ~ (B.3) below) are essentially the same. Though complete theoretical derivation yields Eq. (2.34), this expression is not capable to capture the characteristic of programming language. Therefore, a programming friendly equation, i.e., Eq. (3.6), is needed to actualize out our calculation.

$$\left(\frac{d\sigma}{d\Omega}\right)_{coh\ el} = N\frac{(2\pi)^3}{v_0}\sum_{\boldsymbol{\tau}}\delta(\boldsymbol{\kappa}-\boldsymbol{\tau})\left|F(\boldsymbol{\kappa})\right|^2 . \tag{B.1}$$

$$\downarrow$$

$$\sigma_{el,coh} = \frac{\lambda^2}{2v_0}\sum_{\tau\le 2/\lambda}\frac{1}{\tau}\left|F(\boldsymbol{\kappa})\right|^2 , \text{ where } F(\boldsymbol{\kappa}) = \sum_{\mu}\bar{b}_{\mu}e^{i\boldsymbol{\kappa}\cdot\mathbf{d}}e^{-W_{\mu}} . \tag{B.2}$$

$$\downarrow$$

$$\sigma_{coh}(E,\mu) = \frac{1}{E}\sum_{E_i<E}\frac{f_i}{\tau_i}e^{-4wE_i}\delta(\mu-\mu_i). \tag{B.3}$$

By comparing Eq. (B.1) and (B.2), it can be found that the difference between them is the same as that between (A.4) and (A.7). That is, Eq. (B.1) is the differential cross section per unit cell with fixed neutron momentum change $\boldsymbol{\kappa}=\boldsymbol{\tau}$, while Eq. (B.2) is the total scattering cross section per unit cell with all possible neutron momentum change. By applying the same integral from Eq. (A.4) to (A.7), Eq. (B.2) can be derived from Eq. (B.1).

Starting from Eq. (B.2), by using $E = \pi\hbar/m\lambda^2$ , plugging in $F(\boldsymbol{\kappa})$, and assuming that there exists a universal Debye-Waller factor for all atoms in the unit cell, following derivation can be made

$$\begin{aligned}\sigma_{el,coh} &= \frac{\lambda^2}{2v_0}\sum_{\tau\le 2/\lambda}\frac{1}{\tau}\left|F(\boldsymbol{\kappa})\right|^2 \\ &= \frac{1}{E}\frac{\pi^2\hbar^2}{mv_0}\sum_{\tau\le 2/\lambda}\frac{1}{\tau}\left|F(\boldsymbol{\kappa})\right|^2 \\ &= \frac{1}{E}\frac{\pi^2\hbar^2}{mv_0}\sum_{\tau\le 2/\lambda}\frac{1}{\tau}\left|\sum_{\mu}\bar{b}_{\mu}e^{i\boldsymbol{\kappa}\cdot\mathbf{d}}e^{-W_{\mu}}\right|^2 \\ &= \frac{1}{E}\sum_{\tau\le 2/\lambda}\frac{1}{\tau}\frac{\pi^2\hbar^2}{mv_0}\left|\sum_{\mu}\bar{b}_{\mu}e^{i\boldsymbol{\kappa}\cdot\mathbf{d}}\right|^2 e^{-2W_{\mu}}\end{aligned},$$

while Eq. (B.3) is

$$\begin{aligned}\sigma_{coh}(E,\mu) &= \frac{1}{E}\sum_{E_i<E}\frac{f_i}{\tau_i}e^{-4wE_i} \\ &= \frac{1}{E}\sum_{E_i<E}\frac{1}{\tau}\frac{\pi^2\hbar^2}{N_{\mu}mv_0}\left|\sum_{j=1}^{N}\sqrt{\sigma_j}e^{i\boldsymbol{\tau}\cdot\mathbf{r}_j}\right|^2 e^{-4wE_i}\end{aligned}.$$

Comparing the above two equations, the only difference except the Debye-Waller factor is that Eq. (B.3) from NJOY is calculating averaged total coherent elastic cross section in a unit cell, while Eq. (B.1) from Squires is calculating total cross section from all atoms in a unit cell. The Debye-Waller factor in both equations looks different because of different terminology. This difference can be examined by comparing Eq. (3.1) ~ (3.3) with Eq. (2.38).

NJOY Eq. (3.1) ~ (3.3):

$$\begin{aligned}-4wE &= -4\cdot\frac{\lambda}{Ak_BT}\cdot\frac{\hbar^2\tau^2}{8m_n} \\ &= -\frac{\hbar^2\tau^2}{2M_{\mu}k_BT}\int_0^{\infty}\frac{1}{\beta}\rho(\beta)\coth(\frac{\beta}{2})d\beta\end{aligned}.$$

Squire Eq. (2.38):

By using $\omega = k_B T\beta/\hbar$, $\rho(\omega) = \hbar\rho(\beta)/k_B T$, $d\omega = k_B T d\beta/\hbar$, it can be written that

$$
\begin{aligned}
-2W_\mu &= -2\cdot\frac{\hbar\tau^2}{4M_\mu}\int_0^{\omega_m}\frac{\rho(\omega)}{\omega}\coth\left(\frac{\hbar\omega}{2k_B T}\right)\mathrm{d}\,\omega \\
&= -\frac{\hbar\tau^2}{2M_\mu}\int_0^{\beta_m}\frac{\hbar}{k_B T}\frac{1}{\beta}\frac{\hbar}{k_B T}\rho(\beta)\coth\left(\frac{\beta}{2}\right)\frac{k_B T}{\hbar}\mathrm{d}\,\beta\,. \\
&= -\frac{\hbar^2\tau^2}{2M_\mu k_B T}\int_0^{\infty}\frac{1}{\beta}\rho(\beta)\coth(\frac{\beta}{2})d\beta
\end{aligned}
$$

The two Debye-Waller factors are exactly the same. Therefore, the only difference between Squire's cross section and NJOY's cross section is the first one per unit cell and the second one per atom.

## Appendix C  Discussion of ENDF Format

In this appendix, features of ENDF library are discussed.  It should be addressed to the reader beforehand that this appendix is not intended to substitute the "*ENDF-6 Formats Manual*" published by *National Nuclear Data Center*, *Brookhaven National Laboratory*. What this appendix will do is, a) explain basic structure of ENDF libraries, b) address some of the important parameters in the ENDF libraries, and c) give readers general directions on how to generate ENDF libraries based on NJOY code system.  Readers should understand when talking about ENDF libraries in this work, it is always referred to the *Thermal Neutron Scattering Sublibrary*, which is also called the "*file 7 thermal neutron scattering law data*".

Tables shown in this appendix are parts of an already published *ENDF* library of *Be*.

Table 4. Beginning section of ENDF library.

```
 $Rev:: 570      $  $Date:: 2011-12-16#$                                 1 0  0     0
 1.260000+2 8.934780+0          -1           0           0          a 1  26 1451     1
 0.000000+0 0.000000+0           0           0           0            6  26 1451     2
 1.000000+0 2.000000+7          b1           0          12          c 7  26 1451     3
 0.000000+0 0.000000+0           0           0         d43            3  26 1451     4
 Be metal  LANL       EVAL-APR93 MacFarlane                             26 1451     5
 Ref. 3 (1994)        DIST-DEC06                    20111222            26 1451     6
----ENDF/B-VII.1      MATERIAL   26                                     26 1451     7
-----THERMAL NEUTRON SCATTERING DATA                                    26 1451     8
------ENDF-6 FORMAT                                                     26 1451     9
                                                                        26 1451    10
  Temperatures = 296, 400, 500, 600, 700, 800, 1000, 1200               26 1451    11
                                                                        26 1451    12
 History                                                                26 1451    13
 -------                                                                26 1451    14
 this evaluation was generated at the los alamos national               26 1451    15
 laboratory (apr 1993) using the leapr code.  the physical              26 1451    16
 model is very similar to the one used at general atomic                26 1451    17
 in 1969 to produce the original endf/b-iii evaluations                 26 1451    18
 (see ref. 1).  tighter grids and extended ranges for alpha             26 1451    19
 and beta were used.  a slightly more detailed calculation              26 1451    20
 of the coherent inelastic scattering was generated.  of                26 1451    21
 course, the various constants were updated to agree with               26 1451    22
 the endf/b-vi evaluation of be.                                        26 1451    23
                                                                        26 1451    24
 Theory                                                                 26 1451    25
 ------                                                                 26 1451    26
 the phonon dispersion curves were fitted by Schmunk et al              26 1451    27
 using a model of central forces that extend to the fifth               26 1451    28
 nearest neightbors (ref 2).  the phonon spectrum corresponding         26 1451    29
 to this model was calculated by the root sampling method,              26 1451    30
 and then used to compute s(alpha,beta). the coherent elastic           26 1451    31
 scattering cross section was computed using the known lattice          26 1451    32
 3tructure (hexagonal close-packed) and the debye-waller                26 1451    33
 integrals from the lattice dynamics model.                             26 1451    34
                                                                        26 1451    35
 References                                                             26 1451    36
 ----------                                                             26 1451    37
 1. j.u.koppel and d.h.houston, reference manual for endf thermal       26 1451    38
    neutron scattering data, general atomic report ga-8774              26 1451    39
    revised and reissued as endf-269 by the national nuclear            26 1451    40
    data center, july 1978.                                             26 1451    41
 2. r.e.schmunk, r.m.brugger, p.d.randolph, and k.a.strong,             26 1451    42
    phys. rev. 128,562 (1962).                                          26 1451    43
 3. r.e.macfarlane, new thermal neutron scattering files for            26 1451    44
    endf/b-vi release 2, los alamos national laboratory report          26 1451    45
    LA-12639-MS (ENDF-356) March 1994.                                  26 1451    46
                                                                        26 1451    47
                              1         451        e 50          f 1   26 1451    48
                              7           2        g235          f 1   26 1451    49
                              7           4       14842          f 1   26 1451    50
 0.000000+0 0.000000+0        0           0           0            0   26 1  099999
```

Every ENDF library begins with a description section looks like the one shown above.

The number 26 on the right hand side column denotes the material number for this library. In this case, it is number 26 for *Be*. The number 1451 in the next column refers to the description section of an ENDF library. The right most column is the line number.

The first line of the library gives information on the version of the library and the date the library is published. From line 5 to line 47, there are 43 lines of text description of the library. Line number 099999 given below line 50 indicates the end of a section.

Between line 1 to 4 and line 48 to 50, there are numbers given in the table. These numbers have different meanings and they might be mistakenly outputted by NJOY program. Therefore, it is important for users to check their meaning and write the right number when generating the library. This appendix will only emphasize known parameters that will be probably modified by hand by the user of *NJOY* program.

a. NMOD: Modification number for this material:

   NMOD=0, evaluation converted from a previous version;

   NMOD=1, new or revised evaluation for the current library version;

   NMOD$\geqslant$ 2, for successive modifications.

   NOTE: For a newly generated library, users should put 1. NJOY outputs 0.

b. LREL: Library release number; for example, LREL=2 for the ENDF/B-VI.2 library.

   NJOY default outputs 0, users should change it to 1 for the current library release number.

c. NVER: Library version number; for example, NVER=7 for version ENDF/B-VII.

   NJOY default outputs 6, users should revise it to 7 for the current library version.

d. NWD: Number of records with descriptive text for this material. Each record contains

up to 66 characters.

NJOY default output is 0. Users should change it to number of descriptive lines in this section. In this example, it begins at line 5, ends at line 47. There are 43 lines of records, therefore users should put 43 here.

e. $NC_1$: ENDF reaction designation of the 1st section, which indicates number of lines for the first description section.

Default description section will always be modified, in this sense users must change this number to corresponding line number. In this example, it is 43 lines.

f. $MOD_n$: Modification indicator for the nth section. The value of $MOD_n$ is equal to NMOD if the corresponding section was changed in this revision. $MOD_n$ must always be less than or equal to NMOD.

NJOY default outputs 0. For a new library, change it to 1.

g. $NC_1$: This depends on specific situation. But for a file 7 library, if users made modifications on section 2, i.e., the coherent elastic scattering cross section, users must change this number to corresponding line numbers in section 2.

Table 5. Coherent elastic section of ENDF library.

| | | | | | | | | | |
|---|---|---|---|---|---|---|---|---|---|
| 0.000000+0 | 0.000000+0 | 0 | 0 | 0 | 0 | 26 | 1 | 099999 | |
| 0.000000+0 | 0.000000+0 | 0 | 0 | 0 | 0 | 26 | 0 | 0 | 0 |
| 1.260000+2 | 8.934780+0 | 1 | 0 | 0 | 0 | 26 | 7 | 2 | 1 |
| 2.960000+2 | 0.000000+0 | 7 | 0 | 1 | 149 | 26 | 7 | 2 | 2 |
| 149 | 1 | | | | | 26 | 7 | 2 | 3 |
| 1.592731-3 | 1.50846-16 | 5.219428-3 | 8.395295-3 | 6.370925-3 | 1.837831-2 | 26 | 7 | 2 | 4 |
| 6.812159-3 | 6.157714-2 | 1.159035-2 | 7.195941-2 | 1.433458-2 | 7.195941-2 | 26 | 7 | 2 | 5 |
| 1.565828-2 | 8.891480-2 | 1.725101-2 | 8.891480-2 | 1.955401-2 | 1.105631-1 | 26 | 7 | 2 | 6 |
| 2.087771-2 | 1.139960-1 | 2.202921-2 | 1.403395-1 | 2.247044-2 | 1.597916-1 | 26 | 7 | 2 | 7 |
| 2.548370-2 | 1.636966-1 | 2.724864-2 | 1.692343-1 | 2.999287-2 | 1.692343-1 | 26 | 7 | 2 | 8 |
| 3.070313-2 | 1.742247-1 | 3.521229-2 | 1.874180-1 | 3.653599-2 | 1.916626-1 | 26 | 7 | 2 | 9 |
| 3.812873-2 | 2.160877-1 | 3.981828-2 | 2.160877-1 | 4.114198-2 | 2.311683-1 | 26 | 7 | 2 | 10 |
| 4.290692-2 | 2.383864-1 | 4.503771-2 | 2.486691-1 | 4.636141-2 | 2.519904-1 | 26 | 7 | 2 | 11 |
| 4.697485-2 | 2.585377-1 | 4.856758-2 | 2.770305-1 | 5.334578-2 | 2.883529-1 | 26 | 7 | 2 | 12 |
| 5.733833-2 | 2.900821-1 | 6.069599-2 | 3.021035-1 | 6.255775-2 | 3.090674-1 | 26 | 7 | 2 | 13 |
| 6.785256-2 | 3.317685-1 | 7.245855-2 | 3.506960-1 | 7.635428-2 | 3.612599-1 | 26 | 7 | 2 | 14 |
| 7.804383-2 | 3.629621-1 | 8.218714-2 | 3.724093-1 | 8.326326-2 | 3.823864-1 | 26 | 7 | 2 | 15 |
| 8.811683-2 | 3.880229-1 | 8.988177-2 | 3.947330-1 | 9.784543-2 | 3.982735-1 | 26 | 7 | 2 | 16 |
| 9.892154-2 | 4.097846-1 | 1.019348-1 | 4.170104-1 | 1.071542-1 | 4.289503-1 | 26 | 7 | 2 | 17 |
| 1.135037-1 | 4.343270-1 | 1.145798-1 | 4.465997-1 | 1.175931-1 | 4.532492-1 | 26 | 7 | 2 | 18 |
| 1.228125-1 | 4.593338-1 | 1.290112-1 | 4.691285-1 | 1.368566-1 | 4.745350-1 | 26 | 7 | 2 | 19 |
| 1.408492-1 | 4.873338-1 | 1.489097-1 | 4.893198-1 | 1.498889-1 | 4.931903-1 | 26 | 7 | 2 | 20 |
| 1.592731-1 | 5.096094-1 | 1.681732-1 | 5.103390-1 | 1.697874-1 | 5.110502-1 | 26 | 7 | 2 | 21 |
| 1.703040-1 | 5.142032-1 | 1.759861-1 | 5.180663-1 | 1.801508-1 | 5.219316-1 | 26 | 7 | 2 | 22 |
| 1.894921-1 | 5.219316-1 | 1.927205-1 | 5.307743-1 | 2.034823-1 | 5.320384-1 | 26 | 7 | 2 | 23 |
| 2.062480-1 | 5.392464-1 | 2.135982-1 | 5.422685-1 | 2.244354-1 | 5.433384-1 | 26 | 7 | 2 | 24 |
| 2.271257-1 | 5.436328-1 | 2.277177-1 | 5.465439-1 | 2.293533-1 | 5.497250-1 | 26 | 7 | 2 | 25 |
| 2.427840-1 | 5.516943-1 | 2.502310-1 | 5.559540-1 | 2.637371-1 | 5.566364-1 | 26 | 7 | 2 | 26 |
| 2.658893-1 | 5.568018-1 | 2.659432-1 | 5.574593-1 | 2.691716-1 | 5.612844-1 | 26 | 7 | 2 | 27 |
| 2.848299-1 | 5.616597-1 | 2.897588-1 | 5.619512-1 | 2.900493-1 | 5.651667-1 | 26 | 7 | 2 | 28 |
| 3.054171-1 | 5.656312-1 | 3.057076-1 | 5.663680-1 | 3.121753-1 | 5.678497-1 | 26 | 7 | 2 | 29 |

Numerical modification of this section is needed if the users intend to publish a library by a set of separated libraries. For example, the library of 3C-SiC is generated by two parts, i.e., Si cross section and C cross section. By generating the total coherent elastic cross section for SiC from NJOY, users must divide the cross section by two and put them separately into Si and C libraries. In this example, there are 149 entries for the record of cross section. The record begins at line 4. $1.592731\times10^{-3}$ *eV* is the energy and $1.50846\times10^{-16}$ *barn* is the associated cross section. These two numbers are called an entry for the record. As discussed above, in the 149 entries, users may want to divide the cross section values and put them back at the same place.

Table 6. Inelastic section of ENDF library.

```
0.000000+0 0.000000+0          0          0          0          0  56 7  099999
1.560000+2 5.545400+1          0          1          0          0  56 7  4     1
0.000000+0 0.000000+0          0          0          6          0  56 7  4     2
1.205000+1 9.000000+1 5.545400+1 2.277000+0 0.000000+0 1.000000+0  56 7  4     3
0.000000+0 0.000000+0          0          0          1        151  56 7  4     4
       151          4                                              56 7  4     5
2.000000+1 0.000000+0          5          0          1         82  56 7  4     6
        82          4                                              56 7  4     7
1.008000-2 3.658623-5 1.500000-2 5.416559-5 2.520000-2 9.003682-5  56 7  4     8
3.300000-2 1.169516-4 5.040600-2 1.754297-4 7.560000-2 2.563006-4  56 7  4     9
1.008120-1 3.329191-4 1.512180-1 4.738441-4 2.016240-1 5.994872-4  56 7  4    10
2.520300-1 7.110428-4 3.024360-1 8.096230-4 3.528420-1 8.962633-4  56 7  4    11
4.032480-1 9.719270-4 4.536540-1 1.037510-3 5.040600-1 1.093846-3  56 7  4    12
5.544660-1 1.141709-3 6.097110-1 1.185285-3 6.702590-1 1.223381-3  56 7  4    13
7.366230-1 1.254744-3 8.093490-1 1.278084-3 8.890610-1 1.292143-3  56 7  4    14
9.764350-1 1.295726-3 1.072130+0 1.287792-3 1.177080+0 1.267501-3  56 7  4    15
1.292110+0 1.234322-3 1.418220+0 1.188092-3 1.556330+0 1.129172-3  56 7  4    16
1.707750+0 1.058320-3 1.873790+0 9.768745-4 2.055660+0 8.868250-4  56 7  4    17
2.255060+0 7.904766-4 2.473520+0 6.906767-4 2.712950+0 5.904059-4  56 7  4    18
2.975460+0 4.926975-4 3.263080+0 4.005181-4 3.578320+0 3.163433-4  56 7  4    19
3.923900+0 2.420867-4 4.302660+0 1.789656-4 4.717700+0 1.273938-4  56 7  4    20
5.172560+0 8.699956-5 5.671180+0 5.676854-5 6.217580+0 3.524468-5  56 7  4    21
6.816500+0 2.071799-5 7.472890+0 1.147181-5 8.192280+0 5.949142-6  56 7  4    22
8.980730+0 2.871334-6 9.844890+0 1.280927-6 1.079190+1 5.242693-7  56 7  4    23
1.183030+1 1.951413-7 1.296740+1 6.554923-8 1.421450+1 1.964189-8  56 7  4    24
1.558150+1 5.196621-9 1.707960+1 1.199880-9 1.872080+1 2.38798-10  56 7  4    25
2.052030+1 4.03277-11 2.249220+1 5.69521-12 2.465260+1 6.61494-13  56 7  4    26
2.800000+1 2.32181-14 3.000000+1 3.11776-15 3.200000+1 4.16973-16  56 7  4    27
3.400000+1 5.55723-17 3.600000+1 7.38396-18 3.800000+1 9.78508-19  56 7  4    28
4.000000+1 1.29367-19 4.250000+1 1.02835-20 4.500000+1 8.15176-22  56 7  4    29
4.750000+1 6.44636-23 5.000000+1 5.08709-24 5.250000+1 4.00713-25  56 7  4    30
```

There is nothing known for the users to revise from NJOY output in file 7 section 4. However, one thing to must be reminded to the readers is the $\alpha$ grid which is in the red box shown above appears only once in the library. In the rest of the library, it will implicitly default that all cross sections follow the same $\alpha$ grid.